Efficiency- and lifetime-limiting effects of commercially available UVC LEDs

A review

Onushkin, Grigory; Ruschel, Jan ; Piva, Francesco ; Buffolo, Matteo; Rass, Jens ; Davis, Lynn ; Trivellin, Nicola ; De Santi, Carlo ; van Driel, Willem; Meneghini, Matteo

DOI
10.1088/2515-7647/adebcb

Publication date
2025

Document Version
Final published version

Published in
JPhys Photonics

TOPICAL REVIEW • OPEN ACCESS

Efficiency- and lifetime-limiting effects of commercially available UVC LEDs: a review

To cite this article: Grigory Onushkin *et al* 2025 *J. Phys. Photonics* **7** 032002

Journal of Physics: Photonics

TOPICAL REVIEW

Efficiency- and lifetime-limiting effects of commercially available UVC LEDs: a review

Grigory Onushkin[1,7], **Jan Ruschel**[2,7], **Francesco Piva**[3,7,*], **Matteo Buffolo**[3,6], **Jens Rass**[2], **Lynn Davis**[4], **Nicola Trivellin**[3], **Carlo De Santi**[3], **Willem van Driel**[1,5] and **Matteo Meneghini**[3,6]

[1] Signify, High Tech Campus 48, 5656 AE Eindhoven, The Netherlands
[2] Ferdinand-Braun-Institut (FBH), Gustav-Kirchhoff-Str. 4, 12489 Berlin, Germany
[3] Department of Information Engineering, University of Padova, Padova, Italy
[4] RTI International, Durham, NC, United States of America
[5] Delft University of Technology, 2600 AA Delft, The Netherlands
[6] Department of Physics and Astronomy, University of Padova, Padova, Italy
[7] These authors contributed equally to this work.
[*] Author to whom any correspondence should be addressed.

E-mail: francesco.piva@unipd.it

Keywords: degradation, UVC, performance, reliability, LED, AlGaN

OPEN ACCESS

RECEIVED
19 November 2024

REVISED
11 April 2025

ACCEPTED FOR PUBLICATION
2 July 2025

PUBLISHED
18 July 2025

Abstract

This review is aimed at providing an overview of the technologies of currently-available UVC LEDs, on the challenges that these devices have to face, and on the peculiar features that these modern solid-state emitters exhibit. In particular, this paper is aimed at serving as a bridge between device developers and system manufacturers, by increasing awareness of the differences, both in terms of reliability and operation, that AlGaN-based UVC LEDs show with respect to their visible InGaN/GaN-based counterparts. In this view, this work reports performance and lifetime figures of both commercially-available and research-grade LEDs, showing their limitations in terms of temperature- and current-dependency of the emission spectrum. Both catastrophic and gradual processes that lead to device degradation are discussed, with a particular focus on the kinetics that device properties exhibit during prolonged operation. Moreover, also package-related degradation processes are investigated, which stand-out due to the peculiar structures and materials required to sustain both high-energy UV photons and high localized self-heating, while maximizing the optical efficiency of the LEDs. Ultimately, the data reported within this paper should help the final user in predicting and mitigating degradation effects, while also serving as a reference to manufacturers for the improvement of next generation devices.

Contents

1. Introduction

Light emitting diodes (LEDs) that emit in the ultraviolet (UV) wavelength range can be used in a wide range of applications from material processing and sensing to disinfection and sterilization [1, 2]. Therefore, these emitters have gained considerable interest over the last decade, and their development of commercial UV LED products has shown impressive progress with respect to output power, efficiency, and lifetime [1, 3–5]. These UV-LEDs are based on the AlGaN material system, and the emission wavelength depends primarily on the Al–Ga ratio. In spite of their development, the intrinsic technologies in these semiconductor devices are still not as mature as their InGaN-based counterparts emitting in the visible range, which are widely used for white light applications. For the latter, significant knowledge about the material system, epitaxy, front- and backend processing and packaging has been gained over the last 30 years of research, development, and commercialization. While some of this knowledge can be adopted for UV-LEDs, the shift from the InGaN to the AlGaN material system and the increased photon energy raises new challenges and partly requires new concepts and solutions for commercial market adoption.

The wavelength of AlGaN-based UV-LEDs can be defined in a range of approximately 200–360 nm by the alloy composition, and the chosen wavelength defines the primary application. LEDs in the UVA band, which covers the spectral range from 315 to 380 nm, are primarily used in industrial processes such as ink curing [2]. UV LEDs with emissions above ≈360 nm are mainly based on the InGaN materials system [6]. However, achieving lower wavelength emissions (i.e. <360 nm) requires shifting to the less mature AlGaN epitaxy [1, 3–5, 7, 8]. Fortunately, there is a wide range of potential applications for sub-360 nm sources to help attract commercial interest in developing and optimizing AlGaN technologies. For example, sources emitting in the UVB band, which covers the spectral range from 280 nm to 315 nm, can be used in phototherapy treatments for conditions such as dermatitis and psoriasis. Sources emitting in the UVC band, which covers the spectral range from 200 nm to 280 nm, are garnering significant attention for deactivation of pathogens (e.g. viruses, bacteria, spores, mold) on surfaces, air, and in water [9, 10]. UVC irradiation is effective at pathogen deactivation through several mechanisms including modification of ribonucleic acid and proteins to prevent pathogen replication [9]. The time required for pathogen deactivation depends on multiple factors including source wavelength, source intensity, and source exposure time (i.e. total fluency).

As a result, knowledge of the potential AlGaN structures and the impact of long-term performance parameters such as radiant power maintenance and device reliability is important for designing commercial systems for water purification, air disinfection, and medical treatment utilizing this emerging LED technology in an optimized way. The primary aim of using LED technologies in these commercial applications is to replace conventional mercury vapor discharge lamps, which are a potential environmental hazard due to the use of mercury. A secondary aim of using LED technologies in disinfection and medical applications is to open potential new product opportunities, where use of mercury vapor discharge lamps is not suitable due to size, risk of breakage, or geometric configuration. Furthermore, the wavelength spectrum of discharge lamps is fixed, while the peak wavelength of an AlGaN-based LED can be defined by the Al-content in its active region, enabling additional spectral optimization for various applications.

This review is intended to give a snapshot of currently available commercial UVC LED technology and devices and provide an overview of the performance and reliability that commercial AlGaN-based UVC LEDs now achieve. The review aims to fill the gap between developers (e.g. UVC LED manufacturers) and users (e.g. UVC disinfection system manufacturers), as there are very few publications in particular on the long-term stability of commercially available UVC LEDs. It also aims to create awareness of the challenges and special aspects observed for these emitters, which may be instrumental in the development of optimized UVC LED-based applications such as disinfection systems. Furthermore, it provides an overview of the state of research on the degradation processes, which were investigated in more detail using research samples, with the effects being comparable to those of commercial UVC LEDs. On the one hand, this should help the user to make the degradation effects more predictable and manageable. On the other hand, it may help UVC LED developers to find new ways to improve the LED performance.

1.1. Overview of the tested LEDs

This review mainly focuses on the performance and reliability of commercial UVC LEDs. In part, however, it also draws on knowledge gained from AlGaN-based LEDs that emit in the UVB and UVC range, and that were partly manufactured in research facilities. It compiles data from extensive testing across multiple laboratories and includes results from UVC LEDs from 14 different manufacturers. The different manufacturers are denoted by the letters A through Q throughout (table 1). LEDs from the same manufacturer but different model numbers are assigned a Roman numeral. For example, D-1 and D-2 are two different product models from the same manufacturer, where A-1 and D-1 are products from two different manufacturers. Mainly high-powered LEDs (maximum rated forward current greater than 100 mA) are presented in this study. Reliability test results on these products are presented throughout as an indication of the behavior that may occur with AlGaN LEDs in general. This information provides insights into the impact of LED architecture and package structure on device performance and ultimately reliability. This information is critical for the matching of AlGaN LED technologies with emerging applications in water purification, air disinfection, and medical treatments.

1.2. Forecast of further development of UVC LEDs

This review also outlines areas for improvement of future generations of UVC LEDs, including the reduction of defect densities and of detrimental impurities (e.g. hydrogen), and the optimization of LED packages. As these material issues are addressed, the performance (output power per chip and wall plug efficiency) and reliability of UVC LED will continue to improve. It can thus be assumed that the current performance and reliability gap between UVC LEDs and visible light-emitting LEDs will shrink in the future. While the best available single chip LEDs in the wavelength range of 260–280 nm currently emits up to 140 mW of optical power at WPEs of up to 7.5%, we can expect to see LEDs with several hundreds of mW and 10%–20% WPE in the market in the future. At the same time the R70 lifetime, which is the operation time after which the radiation power reduces to 70% of its initial value, is currently still in the range of a few thousand hours for a majority of UVC LED products on the market, but can be expected to be extended above ten thousand hours, even at elevated temperatures or current densities with further improvements. Furthermore, significant developments in packaging technology will follow. Currently, cavity packages made from ceramic submounts with quartz windows are often used in UV LED packaging; however, the use of cheaper materials in combination with stable low-cost materials for encapsulation and light extraction improvement can be expected. In addition, multi-chip packages will be employed once the thermal management allows this. All these developments will create new applications benefiting from the higher performance and reliability that will promote additional growth in the market.

Table 1. Overview of the tested LEDs, which were tested in various facilities. The operating current recommended by the manufacturers and the absolute radiant power measured are listed (averaged and rounded). Furthermore, the main emission wavelength specified by the manufacturer and the order period are also listed.

Manufacturer	Model	Peak wavelength (nm)	Recommended operation current (mA)	Measured radiant power (mW)	Order period
A	A-1	275	250	122	2021, September
	A-3	275	350	138	2020, September
	A-5	275	350	121	2019, August
	A-6	275	100	35	2021, January
	A-7	265	250	106	2022, March
	A-8	265	250	100	2022, June
B	B-1	265	500	63	2021, September
C	C-1	275	350	53	2021, September
	C-5	280	350	63	2020, January
	C-6	280	350	53	2020, March
	C-7	280	20	4	2018, February
D	D-1	280	350	72	2021, September
	D-2	280	350	47	2019, August
	D-3	280	350	109	2023, April
E	E-1	275	500	105	2021, October
	E-2	275	350	53	2021, January
	E-4	265	350	52	2021, May
F	F-1	275	20	3	2014, September
G	G-1	275	150		2019, January
H	H-1	270	30	7	2019, March
	H-3	275	20	3	2020, June
I	I-1	275	20	3	2014, September
L	L-1	265	250	—	2022, January
M	M-1	265	100	—	2021, January
	M-2	265	150	—	2021, January
O	O-1	275	100	17	2018, April
P	P-1	265	440	47	2020, September
	P-2	265	440	58	2021, May
	P-4	265	440	77	2021, July
Q	Q-1	278	100	29	2023, January

2. Performance of state-of-the-art devices

2.1. Performance before long-term operation

A large number of manufacturers produce AlGaN based UV LEDs emitting in the germicidal disinfection range of 260–280 nm. The LEDs differ in the technology that is used in certain aspects which influence the LED's performance. In this section, typical UVC LEDs from different manufacturing countries, with different templates for the semiconductor layer structure, and different packaging technologies are compared. This non-complete set of LEDs includes manufacturers from the United States of America, South Korea, China, and Japan. The substrate in most cases is sapphire, while one manufacturer uses bulk AlN. The chips are mounted either on a planar package, in a cavity package with a flat glass lid, have a glass lens, or are encapsulated with a polymer resin (see figure 1).

2.1.1. Electro-optical characteristics

In figure 2(a) the measured radiant output power is shown as a function of wavelength for LEDs from a wide range of distributors, operated in continuous wave (CW) mode at their nominal forward current. As can be

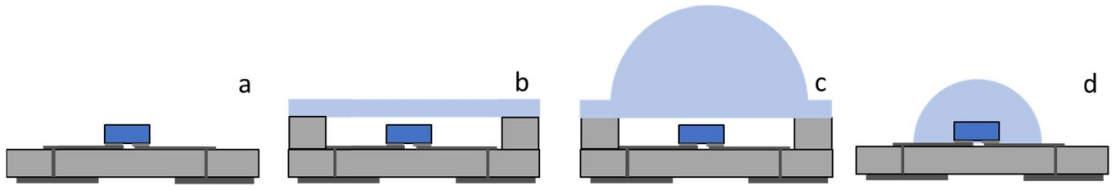

Figure 1. Schematic side view of LEDs in different packages. Left to right: (a): chip on planar submount, (b): cavity package with flat glass lid, (c): chip in cavity package with plano-convex lens, and d: chip on planar submount with encapsulation.

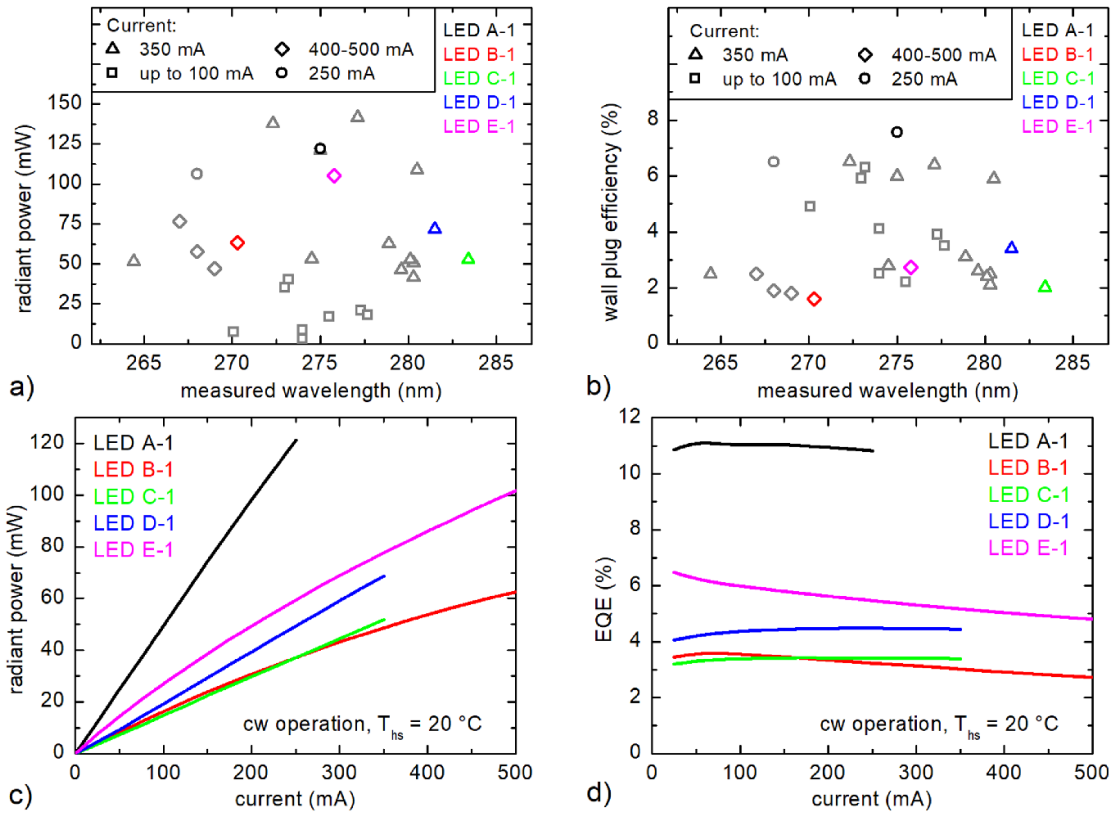

Figure 2. (a) Radiant power vs. wavelength for many different LED types and manufacturers, at varying operation currents. (b) WPE for the same LEDs. (c) Output power vs. current for five selected manufacturers, showing partly deviations from a linear behavior, (d) EQE vs. current for the same LEDs.

seen, the output power varies considerably, with peak radiant powers[8] of up to 140 mW for LEDs emitting at wavelengths of approximately 275 nm and operating at currents of up to 500 mA. To a major extent, this wide range in radiant power is due to significant difference in nominal forward current for the tested UVC LEDs, ranging from 20 mA up to 500 mA. However, the output power comparison is masking the fact that some of the manufacturers can produce LEDs that deliver these radiant powers at considerably higher efficiency, which allows them to operate LEDs at lower currents with reduced energy consumption and heat generation. Such improved performance of UVC LEDs will enable easier designs for the intended applications with significant reduction of cost of ownership and cost of operation. In figure 2(b), the wall plug efficiencies (WPEs) of the same LEDs are compared. Many manufacturers offer WPEs in the range of 2%–4% for their products, whereas some are reaching higher WPE levels of 5%–6%. The highest WPEs approach 7.5%, allowing the generation of 140 mW of 275 nm UVC light at only 250 mA.

The characteristics of the LEDs from five selected manufacturers (labeled A, B, C, D, and E) with different technologies have been further analyzed. Figure 2(c) shows the power-current characteristics of UVC LEDs from these manufacturers at a heat sink temperature (T_{hs}) of 20 °C measured in an integration sphere in 2π configuration up to the respective maximum operating current permitted according to the data sheet. As can be seen, there are three LED types that show rather linear radiant power-current (*PI*)-curves

[8] Radiant power, expressed in watts, is equivalent to radiant flux and to optical power, also referred to as OP.

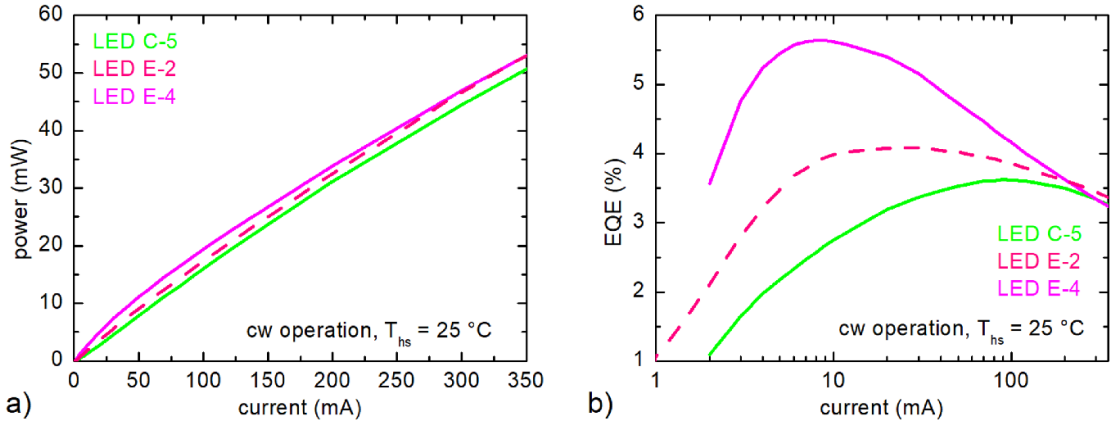

Figure 3. (a) Radiant power vs. current and (b) EQE vs. current for three LEDs with two wavelengths from two different manufacturers showing significant differences in the deviation from a linear power-current curve, especially at low currents (350 mA is the nominal recommended current for these selected UVC LEDs).

while two other LED types show a deviation from the linear behavior at elevated currents. This phenomenon is called droop and is a sign for enhanced non-radiative recombination of charge carriers as a consequence of an increase in temperature or an increase in carrier density at increasing injection currents. By plotting the external quantum efficiency (EQE) as a function of current for these LEDs (see figure 2(d)), it can be seen that the two LED types with the non-linear *PI* curves show a significant reduction of efficiency towards higher current, whereas the other three types have more stable efficiency behavior and therefore deliver optimal performance in a wider range of operating currents, including the designed point of operation.

An even stronger deviation of radiant power vs. current dependence from linearity can often be observed at low operating currents. When plotting the EQE vs. current in semi-logarithmic scale, the maximum can be at different current values, giving additional information on the physical properties limiting the efficiency. This can be seen in figure 3 for selected UVC LEDs from two different manufacturers (green: C-5 (278 nm)) and two UVC LED with different peak emission wavelengths (dark pink dashed: E-2 (265 nm), pink: E-4 (275 nm), offered by same LED manufacturer). A reduction of emission efficiency at different currents can usually be attributed to reduced internal quantum efficiency (IQE) due to an increased non-radiative recombination rate (e.g. Shockley–Read–Hall (SRH) recombination and/or Auger–Meitner recombination processes) and/or a reduced carrier injection efficiency (CIE) [11]. Material properties such as the defect density in the semiconductor layer, barrier heights in the active volume containing the multiple-quantum well (MQW) active region, doping, and carrier confinement due to structures such as electron blocking layers (EBL), can play a role. More insights into the current dependence of efficiency are given in section 3.2.2. Here it is worth mentioning that non-radiative SRH recombination centers are affecting LED efficiency predominantly at lower currents, while Auger–Meitner recombination processes play an essential role at high currents.

The emission spectra of five different UVC LEDs are shown in figure 4. As can be seen, the full width of half maximum (FWHM) ranges from 9.5 to 12.6 nm for center wavelengths between 270 and 285 nm. While this FWHM is wider than the narrow emission peaks seen in mercury discharge lamps and laser diodes, it is a typical value for LEDs emitting in the UV- or violet range while longer wavelengths nitride-based LEDs, e.g. blue (FWHM $\approx$ 20 nm) and green (FWHM $\approx$ 40 nm) show considerably wider emission spectra [12]. When the emission spectra of the LEDs are plotted with a logarithmic scale for the spectral intensity, a parasitic emission at longer wavelength can be seen (figure 4(b)). For UVC LEDs, this broad peak is typically seen at 400–450 nm and it is much weaker than the main peak in the UV-C range, with usually at least two orders of magnitude lower spectral emission intensity at nominal operating currents. The C-1 LEDs show an additional emission shoulder at approximately 320 nm, which is usually a sign for parasitic carrier recombination at the p-side of the AlGaN-heterostructure [13].

2.1.2. Package and far field

The far field distribution of UVC LEDs can differ significantly depending on the chip architecture, substrate choice, package design, presence of an encapsulant or optical lens, and other optical elements such as reflectors embedded into the package. This in turn influences the usability for certain applications, where focused UVC light is beneficial (e.g. for disinfection of water or air within confined spaces along the light beam), whereas a broader beam is useful for reaching better uniformity over exposed surface areas. Figure 5

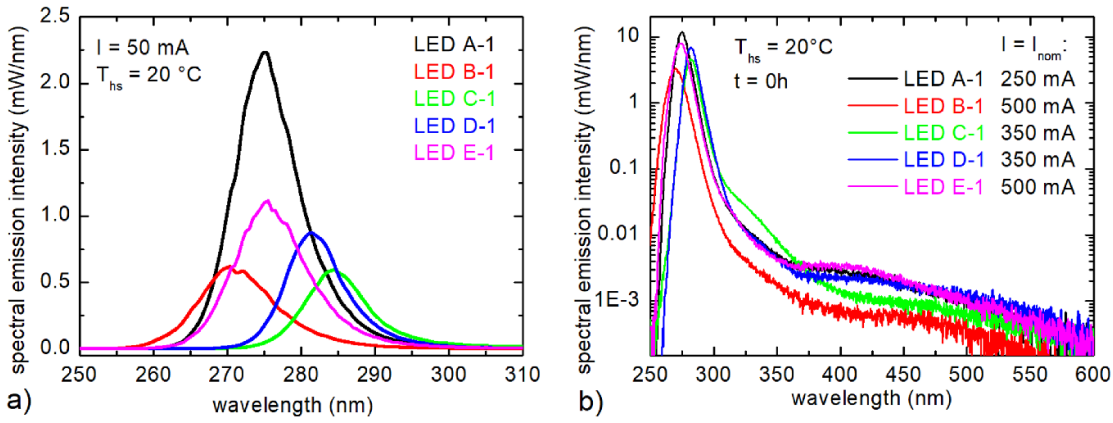

Figure 4. Emission spectra of LEDs from five different manufacturers measured at 50 mA in CW operation in linear scale at 50 mA (a) and in logarithmic scale at the nominal operation current Inom recommended by the manufacturer (b), showing the typical parasitic emission peak in the blue-violet range and an additional shoulder for LED of manufacturer C at about 320 nm.

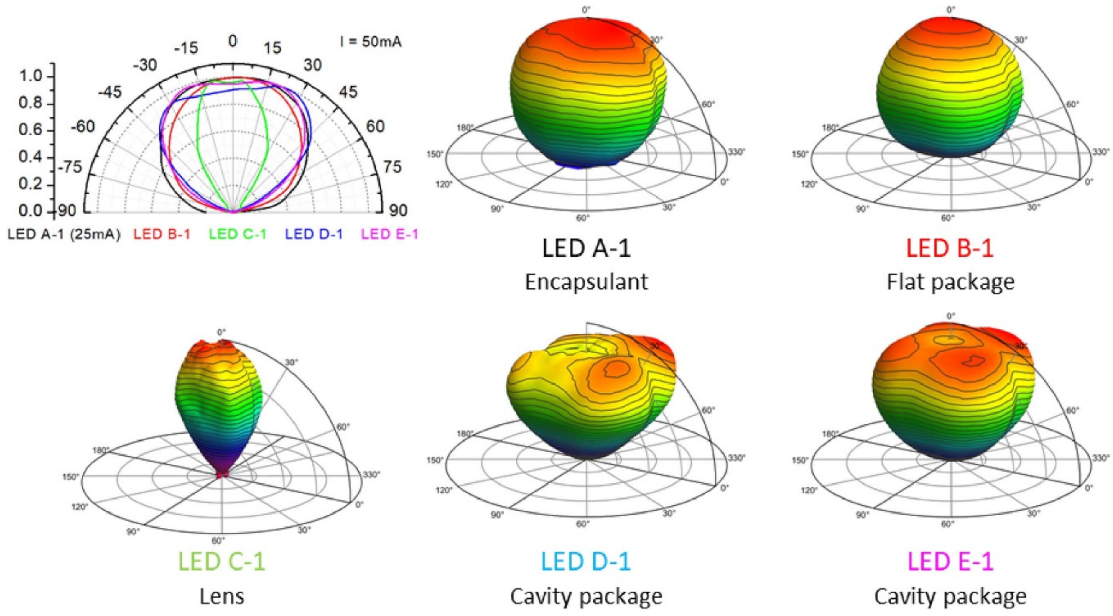

Figure 5. Far field emission pattern of UVC LEDs from five different manufacturers with different packaging techniques (for details, see figure 1.: LED B-1 corresponds to type (a) chip on planar submount, LEDs D-1 and E-1 to type (b)—cavity package with flat glass lid, LED C-1 to type (c) chip in cavity package with plano-convex lens, and LED A-1 to type (d) chip on planar submount with encapsulation).

shows the normalized far field emission distribution as well as line scans through the far field distribution of intensity of LEDs with different packages from five commercial manufacturers. As can be seen, the far field beam angle of LED C-1, which is equipped with a lens, is quite narrow, featuring a FWHM of approximately 60°. Most common LED types are similar to D-1 and E-1, where sapphire-substrate based LED flip-chips are mounted in cavity packages with a planar glass lid (for details, see figure 1: type (b)), and have far field beam angles of approximately 115°. LED type B-1 based on AlN-substrate and flip-chip mounted on a planar package shows a FWHM angle of 120°, and LED A-1, which is flip-chip mounted on a planar package and equipped with an encapsulant shows the largest far field angle of ≈135°. Furthermore, the maximum of the LEDs A-1, B-1, and C-1 is close to 0°, whereas the LEDs D-1 and E-1, with the chip mounted in cavity packages, have a dip at 0° in their far-field distribution and their highest intensity at about 30° to the surface normal. The 3D far field emission has a four-fold symmetry, reflecting the square geometry of the chip inside of the package. These characteristics indicate an enhanced light extraction from the sidewalls and the corners of the chips [14].

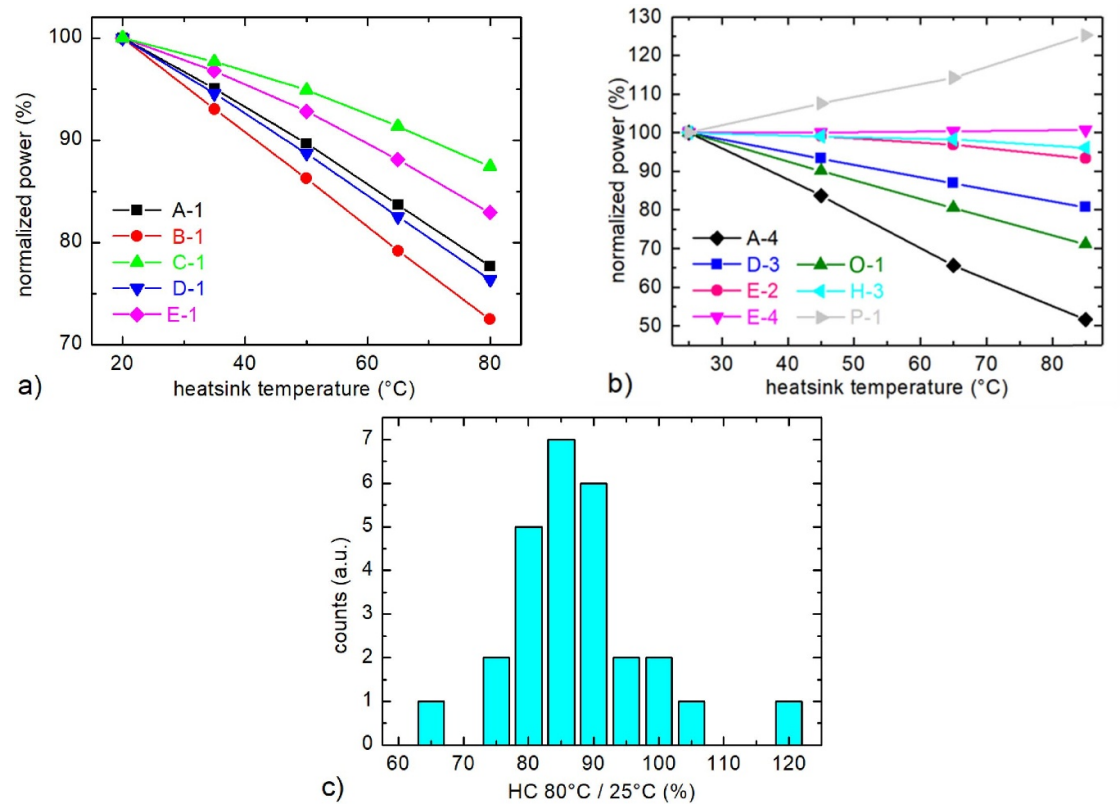

Figure 6. Variation of the radiant output power with the temperature T_{hs} of UVC LEDs from different manufacturers, normalized to 20 °C (a) or 25 °C (b), respectively, and the statistical distribution of the hot–cold factor (c).

2.1.3. Temperature dependence of power, spectra, and linearity

The performance of UV LEDs usually depends strongly on the operating temperature, namely the junction temperature (T_j) of the diode. While T_j is not directly accessible, the technologically more relevant heat sink temperature (T_{hs}) can be easily accessed and controlled in applications.

Figure 6(a) shows the change of the output power of five different LED types in a T_{hs} range of 20 °C–80 °C. The radiant power at nominal operation currents reduces by 13%–28% at a heat sink temperature of 80 °C as compared to the 20 °C operation point. Since the junction temperature is crucial for the efficiency of UVC LED, a high thermal resistance inside of the LED chip, within the package, or at the interface between package and chip can influence the LED performance negatively.

Further analysis of commercial UVC LEDs from other manufacturers shows a large variety of the thermal stability of radiant power. While some show a reduction as high as 50% of relative radiant power when the T_{hs} increases from 25 °C to 80 °C (A-4 in figure 6(b)), others have almost no change in radiant power over temperature (E-2, E-4, I-3). The UVC LEDs from a few manufacturers even showed an increase in radiant power toward higher temperatures (P-1). A figure of merit for the temperature stability is the so-called hot–cold factor (HC), which is defined as the radiant power ratio between 80 °C and 25 °C. As can be seen from figure 6(c), this value is typically in the range between 80% and 90%, with some LEDs showing larger deviations down to 65% or up to 120%. The main mechanisms for the reduction of output power with increasing temperature are the increase in the non-radiative SRH recombination rate and an increased probability for carrier escape from the QW, resulting in the reduction of the overall IQE [15]. An increase in emission power with increasing temperature as seen for device P-1 in figure 6(b) is unusual and it could be related to an improved CIE, if the design of the EBL or the quantum well barriers is not fully optimized for operation at room temperature or below [16]. A deeper insight into the change in electroluminescence (EL) spectra with changes in temperature over a wide range will be given in section 3.2.2.

The T_j value also influences the emission wavelength, since the bandgap of the semiconductor decreases with temperature (band-gap narrowing). Figure 7 shows the change of the peak wavelength of the five commercial LED types normalized to 20 °C at nominal currents. The wavelength increases (red shift) by 0.8–1.6 nm for an increased temperature T_{hs} from 20 °C to 80 °C. The amount of this shift is not correlated to the emission wavelength, the power level change with temperature, or the package technology. Visible blue emitting InGaN-based LEDs are often showing a red shift of the emission peak in the range of 2–3 nm for a

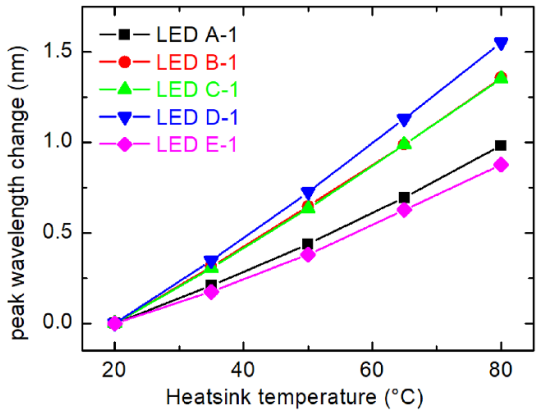

Figure 7. Change of the peak emission wavelength with heat sink temperature of five commercial UVC LEDs normalized to the emission wavelength at 20 °C.

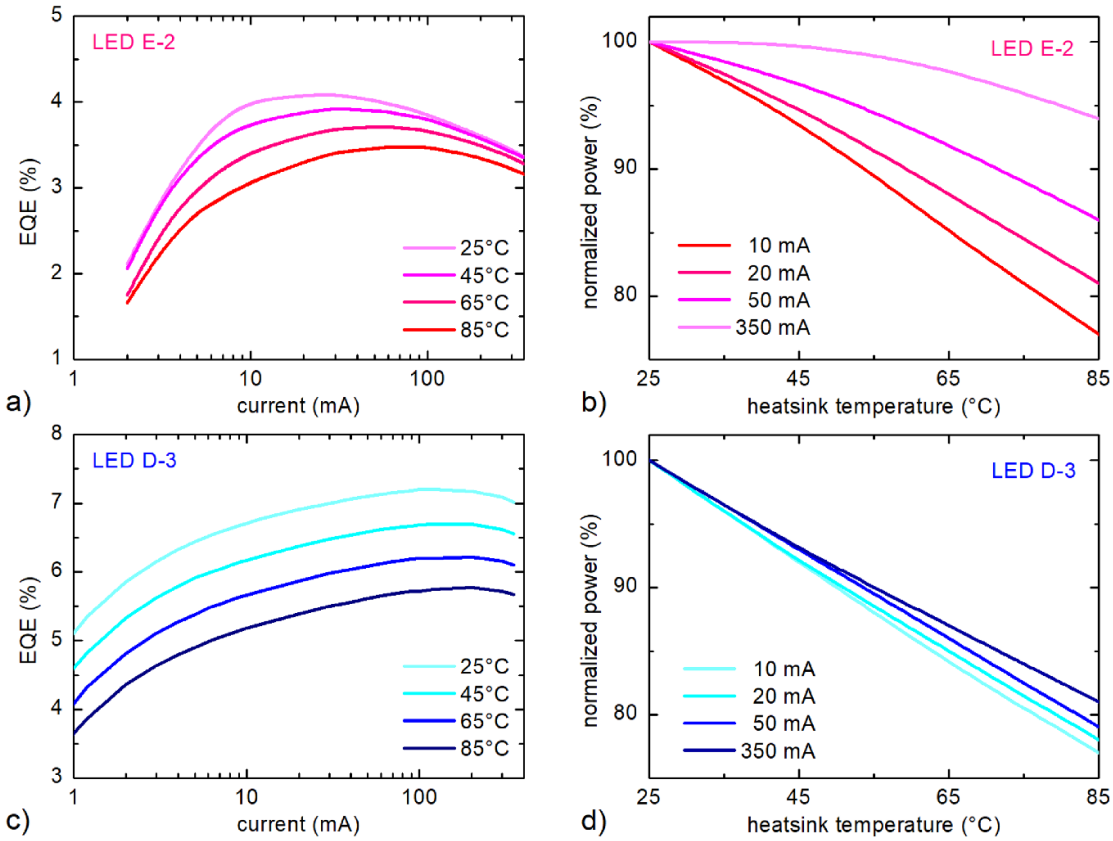

Figure 8. EQE vs. current curves at different T_{hs} (a) and (c) and normalized output power vs. T_{hs} curves at different currents (b) and (d). While the LED of type E-2 (a) shows a strong temperature dependency of the shape of the EQE vs. current curves, LED D-3 ((c) and (d)—bottom) shows almost no change in the shape of the EQE vs. current curves.

similar temperature change from 20 °C to 80 °C. It should be noted that the relative magnitude of the wavelength shift with increasing temperature in relation to the photon energy is similar for UV and visible nitride-based LEDs.

Another property of UVC LEDs that often changes with temperature is the shape of the LED EQE curve vs. current. Typically, UVC LED efficiency (see figures 8(a) and (c)) and radiant power (see figures 8(b) and (d)) decrease with temperature faster for low operating currents, while performance at higher currents could have better temperature stability. The result is that the peak of the EQE curve starts to shift towards higher currents for increased temperatures as shown in figure 8(a). Some recently introduced UVC LED products (type D-3 in figure 8(c)) show limited changes in shape of EQE vs. current trend at elevated temperatures and have small changes in relative radiant power thermal stability at different operating currents (figure 8(d)).

The reason for the change of the radiant power and EQE vs. current curves with the temperature T_{hs} can be attributed to temperature dependency of the radiative and non-radiative (SRH and Auger–Meitner) carrier recombination processes inside of the active region of the LED. In general, a higher T_j increases the rate of non-radiative SRH processes, thus shifting the maximum of the EQE-vs-current curve towards higher currents (see section 3.2.2) [17].

2.2. Degradation of UVC LED chips

This section is intended to provide an overview of typically observed degradation effects during long-term operation of commercial UVC LEDs. As little or no manufacturing and structural details are available for commercial UVC LEDs, it is difficult to determine the physical processes of these LEDs in detail. For this reason, section 3 provides an overview of the state of research behind the degradation processes in research samples that show very similar effects and for which the details are known.

2.2.1. Definition of lifetimes and sudden failures

During long-term operation of UVC LEDs at constant current, degradation mechanisms typically cause the radiant power to decrease over time. A fundamental distinction must be made between two effects that are associated with the reduction in radiant power.

The first effect is a continuous gradual degradation, which is also termed radiant flux depreciation, where the radiant power changes continuously. The gradual degradation can typically be observed by the gradual decrease in the radiant power during constant current operation. The associated lifetime Rx (also referred to as Lx in some references) is defined as the operation time t after which the radiant power $OP(t)$ drops to a relative value $0\% < x < 100\%$ in relation to the initial radiant power $OP(0)$. Typically, the R70 lifetime (operation time after which the radiant power drops to $x = 70\%$) is determined to compare LEDs with regard to the long-term stability of their radiant power. Nevertheless, if the R70 lifetime is too long to be measured experimentally, the usually shorter R90 lifetime, for example, can also be determined in order to compare LEDs. If the degradation dynamics of the investigated LED are known, then extrapolation or accelerated aging experiments can also help to determine the lifetime (see section 3.1.1).

The second effect is catastrophic failure (CF) which occurs when the radiant power drops significantly and abruptly. Often the affected LED no longer emits any radiation at all after a CF event. The LED is usually short-circuited or partially short-circuited after a CF event. A CF event is thus typically accompanied by a significant drop in the operating voltage. The causes of CF events can be complex. For example, a crack in the insulator or macroscopic defects in the semiconductor structure can lead to this type of behavior. In their work, Chen *et al* [18] concluded that hillock epitaxial defects could act as the primary leakage paths in UVC LEDs. The time of a CF event is difficult to predict for an individual LED. Nevertheless, a statistical frequency can be described mathematically (see section 3.1.2).

Extrinsic factors, such as electrical over-stress (EOS) or electro-static discharges (ESDs) can also lead to CF, due to the excessive thermal dissipation, electric field or energy pulse sustained by the device. Specifically, when excessive current density is being concentrated in a small local area, this can cause localized damage to the LED chip. UVC LEDs are found to be more sensitive than visible LEDs to EOS in forward direction, due to limited electrical conductivity of AlGaN semiconductor, and at reverse voltage bias, due to high concentration of defects in the epitaxial layers (e.g. dislocations or point defects). Zener diodes are used in UVC LED packages to protect UVC LED chip from reverse EOS, and in particular ESD events. Additional protection should be considered for UVC LED-based luminaire to reduce the risk of CFs of UVC LEDs from forward-current EOS [19, 20].

2.2.2. Degradation at nominal operation point

To investigate the stability of UVC LEDs under constant current operation, UVC LEDs from 5 chosen representative manufacturers were operated for at least 1000 h. Each batch consisted of 15 LEDs which were operated at recommended currents from the datasheet and at a temperature of $T_{hs} \approx 25\,^{\circ}\mathrm{C}$. The relative change in the radiant power was tracked as irradiance levels measured by SiC photodiodes (as described in [21]), and the averaged values are depicted in figure 9(a). All tested LEDs have in common that their averaged relative radiant power drops noticeably below 100% within 1000 h of operation. However, it is also apparent that the radiant power of the LEDs from the selected representative manufacturers drops by varying degrees within 1000 h of operation. While the radiant power of LED A-1 gradually drops to 90% of the initial value within 300 h of operation, LEDs B-1, D-1 and E-1 still have a relative power of ≈95% after 1000 h operation. The LEDs mentioned so far show gradual degradation in the optical power, also referred to as radiant flux depreciation. A different behavior can be observed for C-1 LEDs, where CF occurs after about 90 h of operation. After a CF, the operating voltage and emission power of the affected LED drops significantly (often even to zero) and abruptly. This results in a stepwise drop of the average radiant power in

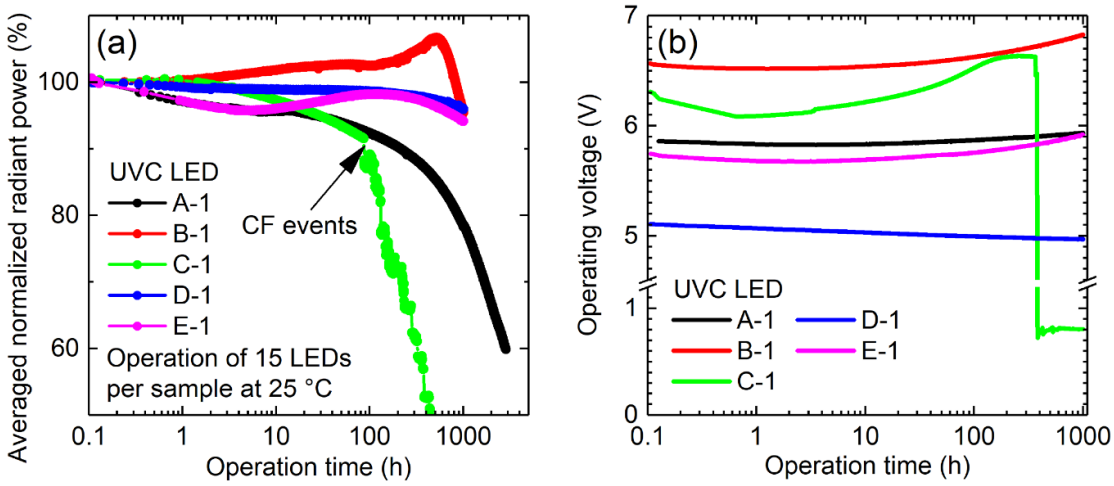

Figure 9. Relative radiant power averaged over 15 LEDs per LED type (a) and typical operating voltage (b) of one representative LED per LED type over operation time. The LEDs were operated at a T_{hs} value 25 °C and at recommended current from the data sheets.

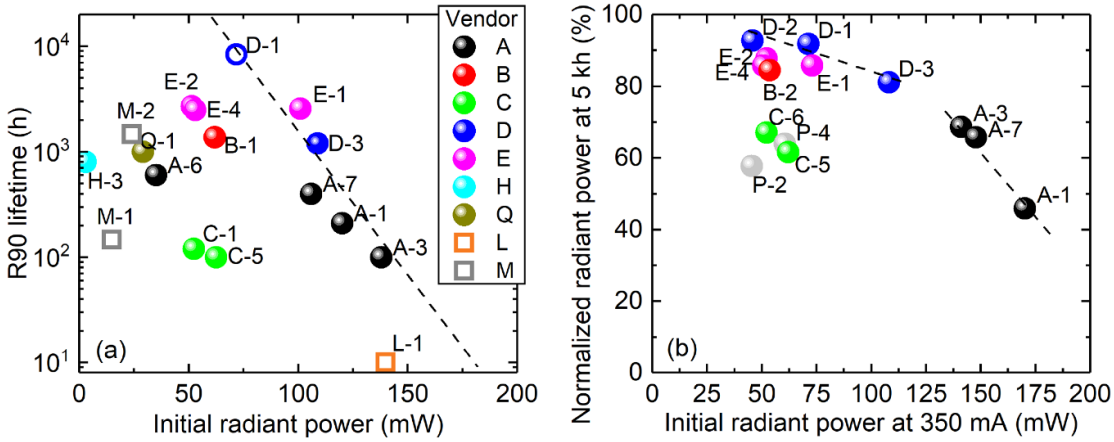

Figure 10. (a) R90 lifetime versus initially measured radiant power at recommended CW currents from the data sheet and at $T_{hs} \approx 25$ °C. The radiation power measurements were carried out under the same conditions as the long-term operation. Only values for UVC LEDs ordered between 2020 and 2023 with a recommended operating current of between 100 mA and 500 mA are shown. Open circles correspond to extrapolated values using the logarithmic function in equation (3.1) from section 3.1.1. Open squares correspond to LEDs for which the radiant power was estimated from the data sheet. (b) Relative radiant power (averaged over the five tested LEDs) after 5000 h of operation at 350 mA and 25 °C versus the initially measured radiant power under the same operation conditions.

the case of the 15 tested C-1 LEDs (figure 9(a)). Due to the accumulation of CFs, the average value of relative radiant power of C-1 LEDs drops to a value <90% within 100 h of operation. Because the drop in the radiant power happens suddenly and because the time of failure is often unpredictable for the individual LEDs, CFs have a completely different character and origin compared to gradual radiant power degradation.

In addition to the radiant power, also the operating voltage typically changes during long-term operation (figure 9(b)). The voltage can increase or decrease over time. In the case of gradual degradation, the observed operating voltage changes were mostly limited to <0.3 V. In the case of a CF event, however, the voltage typically drops significantly, which can be seen for the C-1 LEDs.

Overall, the curves in figure 9(a) show that the R90 lifetimes (operation time after which the radiant power reduces to 90% of the initial value) of the tested LEDs differ greatly and can vary by more than one order of magnitude. This is even more evident in figure 10, where the R90 lifetimes of a larger selection of UVC LED manufacturers (including different models from the same manufacturer) have been plotted versus the initial measured radiant powers. The depicted radiant powers were always measured under the same operating conditions under which the LEDs were aged. In addition, the operating conditions correspond to the recommendations in the manufacturers' data sheets. As some of the R90 lifetimes were long and not all experiments could run for a corresponding length of time, some points were extrapolated (open circles)

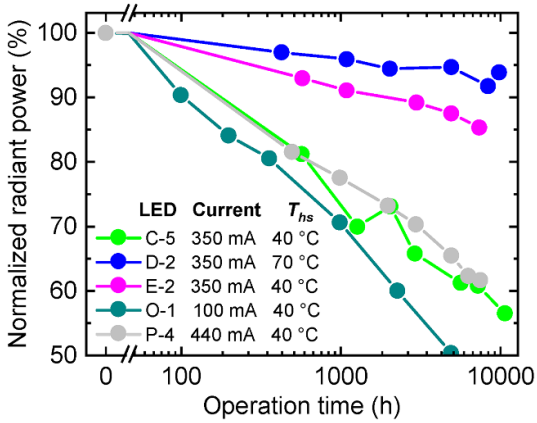

Figure 11. Example of up to 10 000 hours long-term stability trends for relative radiant power measured for several UVC LED products stressed at recommended nominal currents from the data sheet (detailed stress conditions per LED are given in the graph).

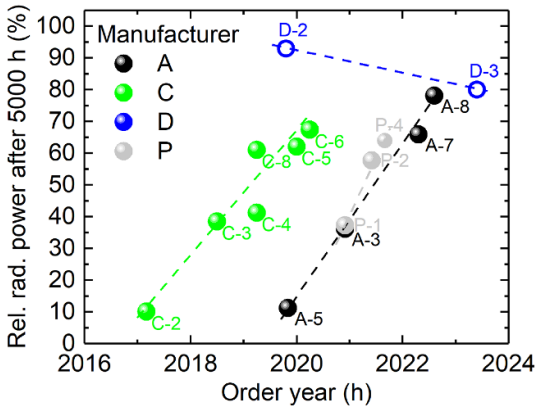

Figure 12. Normalized (to 0 h) radiant power of different UVC LEDs after 5000 h of operation at recommended currents from the data sheets and at heat sink temperatures of $T_{hs} \approx 40$ °C (closed circles) and $T_{hs} \approx 70$ °C (open circles).

using the logarithmic function in equation (3.1) (from section 3.1.1). On the one hand, figure 10(a) shows how widely the emission power and R90 lifetimes of state-of-the-art UVC LEDs can vary. On the other hand, it can also be seen that there is a negative trend for the highest values of lifetime and emission power (dashed line). This means that LEDs with the highest initial radiant power have a comparatively short R90 lifetime (degrade faster) and vice versa. A similar trend can also be seen in figure 10(b) where the relative radiant power after 5000 h of operation at 350 mA and T_{hs} value 25 °C is plotted versus the initially emitted radiant power. The depicted values were measured on different generations of UVC LEDs from manufacturer D and A. Possible reasons for such a negative correlation are discussed in section 3.2.

In addition to the LEDs already shown (figure 9), additional commercial UVC LEDs (partly from the same manufacturers) were operated at constant current for even longer periods (up to 10 000 h). A smaller number of five LEDs was tested for each LED type. The corresponding averaged normalized radiant power is depicted in figure 11 over time. The radiant power of LEDs C-5, O-1 and P-4 reduces to values below 70% in the long-term test, resulting in R70 lifetimes of 1000–4000 h. In contrast, LEDs D-2 and E-2 are more stable, as their radiant power still remains at values >80% at the end of the test period. It can be concluded that these LEDs have an R70 lifetime of >10 000 h.

General trends with significant improvements in UVC LEDs lifetime stability over the past 6 years can be seen from figure 12, where points of same color and dashed trendlines are capturing evolutional improvements of relative radiant power stability levels achieved after 5000 h of operation for UVC LED product generations per each of selected manufacturer.

The different UVC LEDs were ordered in a time period from 2017 to 2023. For most of the investigated manufacturers the results indicate that the relative radiant power after long-term operation, and thus the stability, increased over the years.

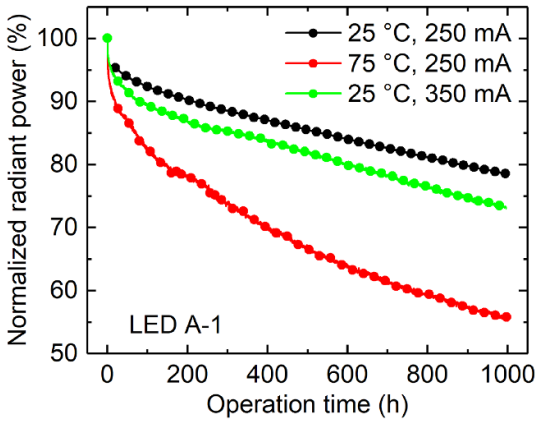

Figure 13. Radiant power of exemplary UVC LEDs from one manufacturer (A-1). The LEDs were operated at different conditions and the radiant power was averaged over 15 LEDs (from $T_{hs} \approx 25$ °C at 250 mA) and over 10 LEDs (for $T_{hs} \approx 25$ °C at 350 mA and for $T_{hs} \approx 75$ °C at 250 mA).

It can be noticed, that recent progress in UVC LED technology achieved by various UVC LED manufacturers enable them to offer to the market UVC LEDs with reasonable levels of long-term (e.g. 5000 h) relative radiant power stability within range of 60%–90%. Availability of these UVC LEDs on the market supports design and release of various emerging UVC LED-based disinfection applications.

2.2.3. Degradation at elevated temperature and increased currents

To study the impact of the operating temperature and the operating current on the degradation of the radiant power, for each of the UVC LEDs shown in figure 9, additional batches of 10 LEDs were operated at changed conditions. In the first experiment, the temperature $T_{hs} \approx 25$ °C was left unchanged and 10 LEDs per manufacturer were operated at an elevated current, which was 1.4 times as high as the recommended current ($1.4 \times I_r$). In the second experiment, 10 LEDs per manufacturer were operated at an elevated temperature of $T_{hs} = 75$ °C, while the current was left unchanged and corresponded to the values recommended in the data sheet (I_r). The radiant power measurements were performed at currents and heat sink temperatures equal to the respective stress condition. The relative radiant power was averaged for each experiment and the values were compared with the data from figure 9.

The results are exemplarily shown for the LED A-1 in figure 13. This example shows that both an increased operating current and an increased operating temperature accelerate the decrease in radiant power over time. Under the conditions tested, operation at $T_{hs} \approx 75$ °C led to the fastest decrease in radiant power in this example. However, it should be noted that the operating current was only increased 1.4 times here. A greater variation of the operating current could possibly have a significantly greater influence on the drop in radiant power over time.

To get an overview of how much the current-accelerated degradation varies from manufacturer to manufacturer, the R90 values were determined for the first experiment. The corresponding averaged values are plotted in figure 14. For all five LED types, the R90 lifetime reduces when the operation current increases. In most cases (A-1, D-1, E-1), the R90 lifetime is shortened by factors between 2.5 and 5. However, a 20-fold shortening was found for LEDs of type B-1. For the special case of C-1 LEDs, it must be mentioned once again that the gradual decrease is superimposed to the occurrence of CF events, which usually have a different cause. Therefore, the measured current-accelerated reduction in R90 lifetime by a factor of ≈6 is not representative for C-1 LEDs.

To get an overview of how the heatsink temperature T_{hs} affects the degradation rates from manufacturer to manufacturer, the R90 values were determined for the second experiment. The corresponding averaged R90 values are shown in figure 15. Here, as well, the R90 reduces for all 5 LED types when the heat sink temperature T_{hs} increases. In most cases (A-1, B-1, E-1), the R90 lifetime is shortened by factors between 11–17. However, an around 40-fold reduction was found for LEDs of type D-1. For the C-1 LEDs, the measured reduction in R90 lifetime by a factor of ≈3 is again not representative due to the superimposition of CF events.

Ten samples of recently manufactured Q-1 UVC LEDs were split into two batches and tested at elevated temperatures of $T_{hs} \approx 65$ °C and at two significantly different operating currents, 50 mA and 150 mA, where 50 mA is half of the typical operating current and 150 mA is the maximal operating current for this LED type, according to the datasheet specification from the manufacturer. It is worth mentioning that this tested

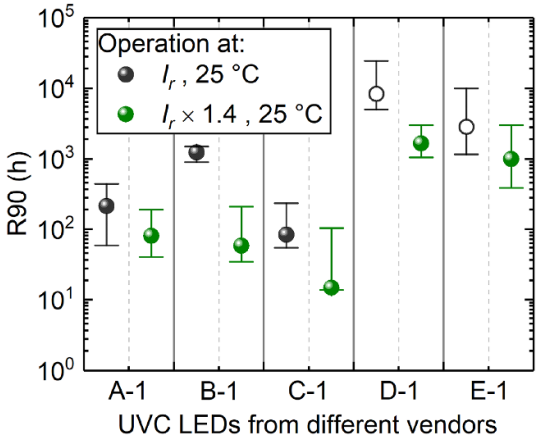

Figure 14. R90 lifetime for an accelerated lifetime test at $T_{hs} \approx 25$ °C at reference operation current I_r (black circles) and at elevated current $I_r \times 1.4$ (green circles) for UVC LEDs from 5 different manufacturers. Open circles correspond to extrapolated values and error bars correspond to the maximum and minimum values measured in the sample batch.

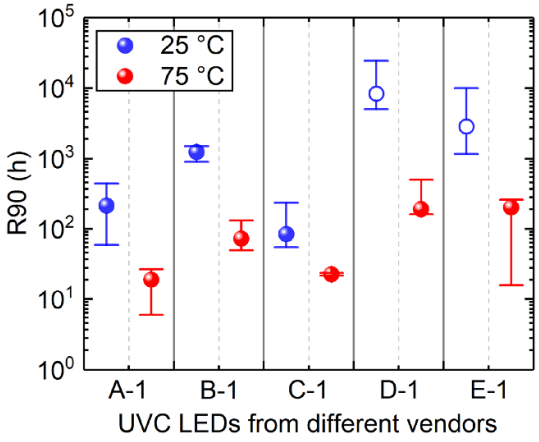

Figure 15. R90 lifetime for an accelerated lifetime test at reference operation current I_r at $T_{hs} \approx 25$ °C (blue circles) and at $T_{hs} \approx 75$ °C (red circles) for UVC LEDs from 5 different manufacturers. Open circles correspond to extrapolated values and error bars correspond to the maximum and minimum values measured in the sample batch.

LED has a relatively small chip size which results in a relatively high nominal current density through the p–n junction which is estimated to be ≈140 A cm^{-2} at the maximum current of 150 mA. Figure 16(a) shows the measured normalized radiant power over time, which were used to determine the R80 and R90 lifetimes. As depicted in figures 16(b), a decrease in R80 and R90 lifetimes by a factor of 5.5x and 7.2x, respectively, can be observed when the operating current is elevated by a factor of 3 (50 mA vs. 150 mA).

2.2.4. Increasing non-linearity of L-I curve (dimmability)

As shown in the previous section, the radiant power measured under nominal operating conditions decreases over time due to degradation. However, the extent of the relative decrease in the radiant power after long-term operation can vary for different measurement currents. The *P–I* curves before and after long-term operation typically show a behavior as depicted in figure 17(a), where the curve shows a stronger relative radiant power loss at low measurement currents. The *P–I* curve is drooping at low measurement currents, causing the *PI* characteristic to lose linearity. The change in this characteristic has an influence on the dimmability of the LED. The extent of the relative decrease in the radiant power at different measurement currents can be calculated by dividing the *P–I* curves after long-term operation by the initially measured *P–I* curves (figure 17(b)). The diagram shows the relative decrease in radiant power averaged over 15 LEDs of types A-1, B-1, D-1, and E-1 before and after 1000 h of operation at recommended currents from the data sheet and at a heat sink temperature of $T_{hs} \approx 25$ °C. The results for LED C-1 are not shown due to the high amount of CFs. The non-linearity of the *PI* curves can be different for the various LEDs. While the output of LED D-1 is relatively constant and decreases only slightly, LED B-1 shows a very pronounced non-linearity of

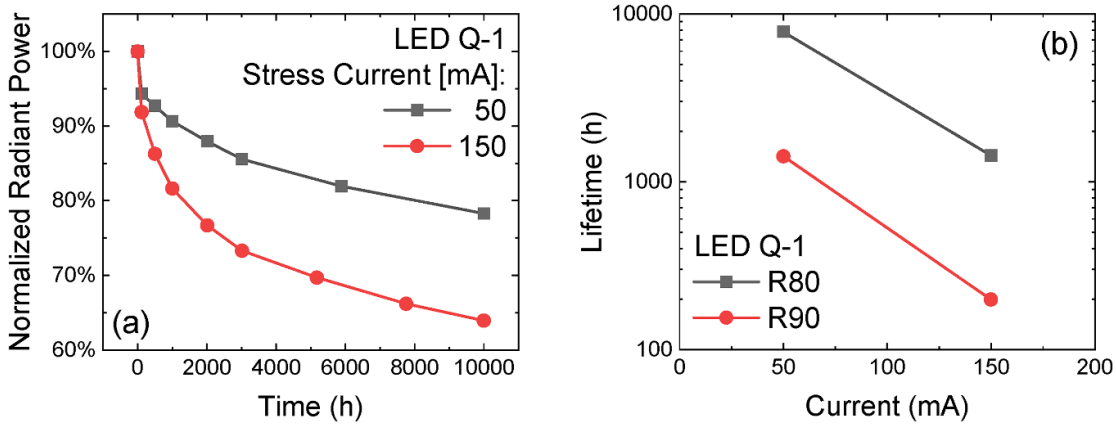

Figure 16. (a) Normalized radiant power vs. stress time of UVC LEDs from one manufacturer (Q-1). The LEDs were operated at two different currents (50 mA and 150 mA) and T_{hs} of 65 °C. (b) Determined lifetimes R80 and R90 for Q-1 UVC LEDs vs. operating stress current.

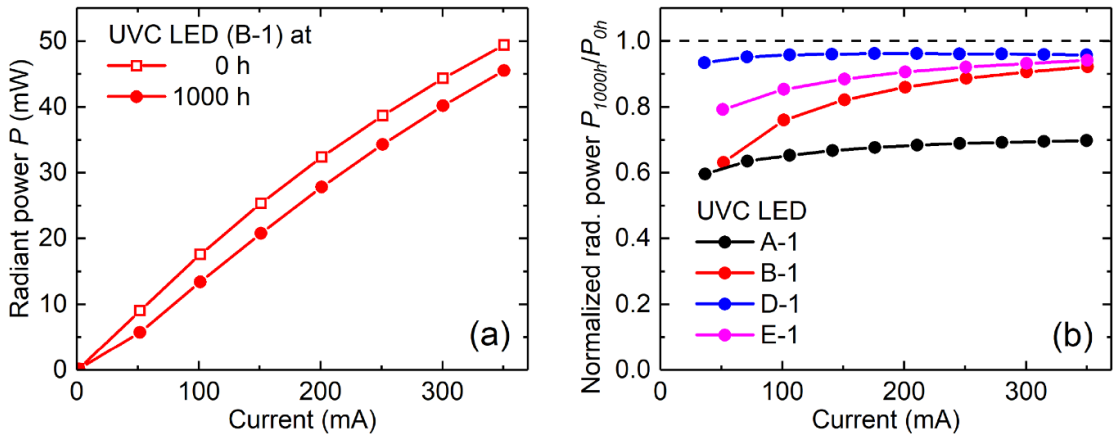

Figure 17. Radiant power versus current characteristics (*PI* curves) of LED B-1 before and after long-term operation (a). Relative radiant power reduction versus current calculated by dividing the *PI* curves after 1000 h by the initially measured *PI* curves (b).

the *P–I* curve. Overall, the relative decrease in radiant power is typically greater at low measurement currents (<150 mA) compared to higher currents.

The above-mentioned non-linearity of radiant power vs. operating current is affected not only by the UVC LED chip design and operating temperature during initial operation, but it also changes substantially over time during continued long-term (few thousand hours) LED operation. Figure 18(a) shows the change of the shape for EQE vs. current curve during operation of UVC LED D-2 under 350 mA (T_{hs} = 65 °C) operation for 430 h, 1100 h, 2065 h, 5024 h, and 8555 h, respectively. It means that the dimming behavior of radiant power vs. current (relative to nominal operating current) will change over time for UVC LEDs. Such changes in dimmability show some similarities to visible green LEDs [22], UVA LEDs [6] and previously studied UVB, UVC LEDs [23]. On the other hand, the observed trend for UVC LED is quite different than that of state-of-the-art white, blue, or red visible LEDs, where the efficiency in relation to the current often does not change significantly over operation lifetime. For almost all tested UVC LEDs, the efficiency at lower dimming (or measurement) currents (I_{meas}) degrades faster than at higher currents (see figure 18(b)). This higher level of efficiency degradation at lower currents can be attributed to a gradual increase of the density of non-radiative recombination centers (NRRCs) within the active region of UVC LED chips over time. It can be expected that higher concentration of NRRCs could have stronger effect on the drop in performance at low currents, while the impact on UVC LED performance at higher measurement currents will be limited (see also section 3.2.2).

Changes in dimming trends for UVC LEDs during operation is another essential aspect for predicting UVC LED behavior and performance in applications, especially where UVC LEDs should be operated in dynamic responsive mode, delivering variable power levels on demand to meet the disinfection need while minimizing energy use.

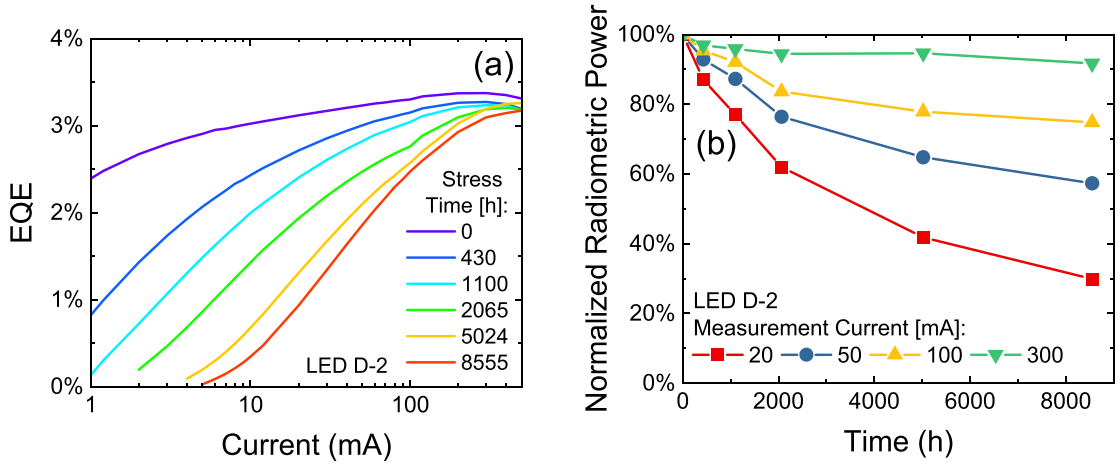

Figure 18. Change in (a) EQE and (b) normalized radiant power versus current for LED D-2 operated at 350 mA and $T_{hs} = 65\ ^{\circ}C$ at different time intervals.

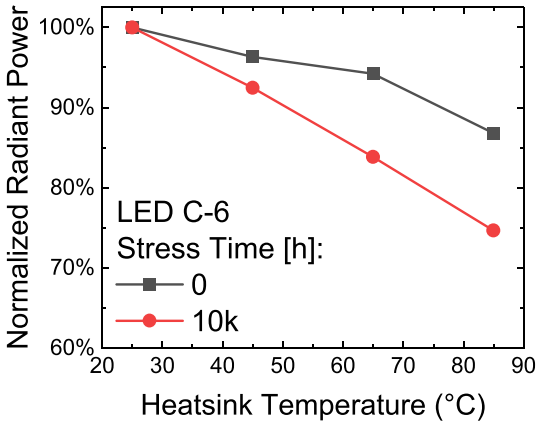

Figure 19. Change in thermal dependence of relative radiant power before and after 10 khours long-time operation for same UVC LED C-6.

2.2.5. Increasing temperature sensitivity

It has been observed that not only non-linearity of radiant power vs. operating current is changing during operation of UVC LEDs, but also the temperature (T) dependency of the radiant power can change. The UVC LED C-6, which was operated for 10 000 h (at $T_{hs} = 65\ ^{\circ}C$ and $I_{stress} = 350$ mA) is an example of such a changing T-dependency of the emission power (figure 19). Further evaluations indicate that there is a correlation between the change in the T-dependency of the radiant power and the non-linearity of the radiant power vs. current characteristics during long-term operation. This means, the more the EQE changes (attributed to stronger impact from NRRCs over time), the stronger is the reduction of thermal stability.

To quantify the change in the temperature dependency, UVC LEDs were measured at two different heat sink temperatures ($T_{meas} \approx 25\ ^{\circ}C$, $T_{meas} \approx 85\ ^{\circ}C$) before and after long-term operation at recommended operating current and at a constant heat sink temperature of $T_{hs} = 65\ ^{\circ}C$ (C-6, D-2, Q-1) and $T_{hs} = 35\ ^{\circ}C$ (P-4, A-7), respectively. The temperature dependent radiant power after long-term operation was then divided by the initially measured temperature dependent radiant power for the respective temperatures $T_{meas} \approx 25\ ^{\circ}C$ and $T_{meas} \approx 85\ ^{\circ}C$. The resulting normalized radiant powers are shown in figure 20 for five different UVC LEDs. It can be seen that some of the tested UVC LEDs (P-4, C-6, A-7) show significantly lower normalized radiant powers at higher measurement temperatures T_{meas} compared to the lower measurement temperature of $T_{meas} = 25\ ^{\circ}C$. Thus, the temperature dependency of their radiant power changed over the long-term operation. In contrast, the temperature dependency of LED D-2 and Q-1 has changed only slightly. Even if this effect is negligible for some LEDs, this study showed that the change in temperature dependency can lead to a deviation of up to 25%. This effect should therefore always be taken into account when drawing conclusions about the radiant power at a specific point in time from degradation curves, which are often recorded at 25 °C [24], especially if the measurement temperature T_{meas} deviates

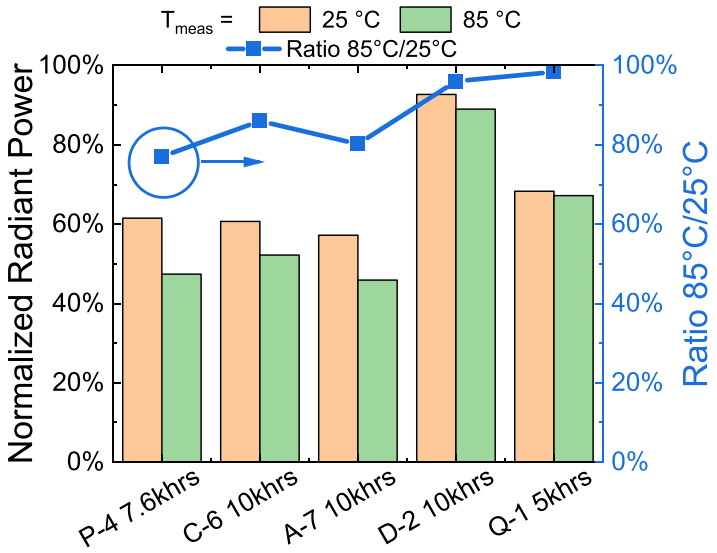

Figure 20. Normalized radiant power measured for five different UVC LEDs at two different temperatures $T_{meas} = T_{hs}$ after long-term operation. The blue squares correspond to the ratio of the normalized power at 85 °C to the normalized power at 25 °C. They are a measure for the change in temperature dependence of the power.

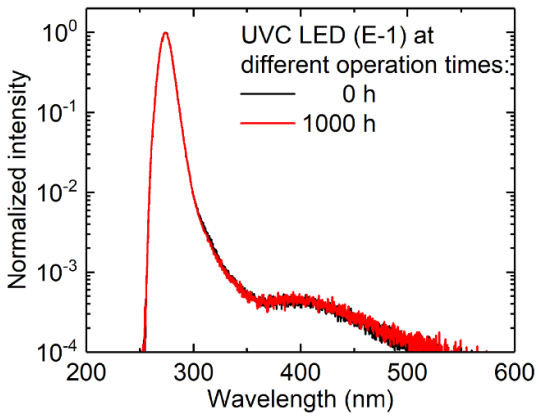

Figure 21. Representative intensity spectra of a UVC LED (E-1) before and after 1000 h operation at 500 mA and $T_{hs} \approx 25$ °C. The spectra were normalized to the intensity maximum and were measured at 500 mA and 25 °C (heat sink temperature).

from the temperature T_{hs} in the degradation experiment. More insight into potential causes for the temperature dependency of the radiant power will be given in section 3.2.2.

2.2.6. Changes in spectrum—parasitic luminescence and peak wavelength

To investigate whether the spectral characteristics of commercial UVC LEDs change during operation, the emission spectra of UVC LEDs (A-1, B-1, C-1, D-1, E-1) were measured before and after 1000 h of operation using an integrating sphere. The measurements and the long-term operation were carried out at a temperature of $T_{hs} \approx 25$ °C and at a current recommended in the respective data sheet. In each case, the integral intensity decreased as shown in figure 9. To compare the shape of the spectra, the measured spectra were normalized to their intensity maximum and plotted in semilogarithmic scale, as shown as an example in figure 21. Within the measurement accuracy ($\Delta\lambda = 0.5$ nm), no shift in the emission maximum was detected for any of the tested LEDs. Relative to the main emission peak, no significant change in the intensity of the parasitic luminescence (intensity at wavelengths >350 nm) could be detected either. In addition, the intensity of the parasitic luminescence before and after 1000 h of operation remained more than two orders of magnitude lower than the intensity of the main emission peak for all LEDs tested under recommended operating current conditions. It can therefore be concluded for the tested UVC LEDs that the shape of the spectra does not change within 1000 h of operation under recommended conditions. Absence of changes in spectral shape for UVC LEDs means that effectiveness (and safety) aspects in UVC LED applications remain unchanged over time. However, if the spectral characteristics are measured at very low currents ($\ll I_r$), the

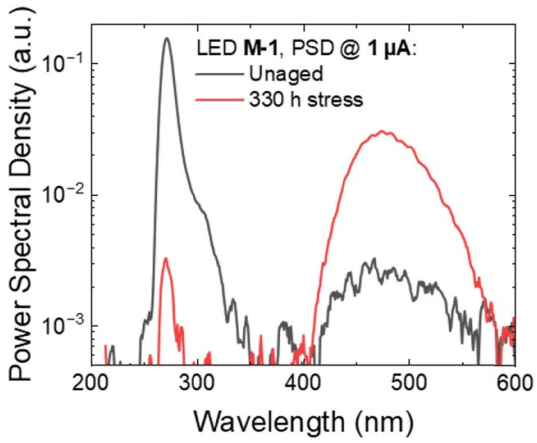

Figure 22. Power spectral density of LED type M-1 measured at a low current level of 1 μA, before and after a constant current stress of 330 h at its absolute maximum current.

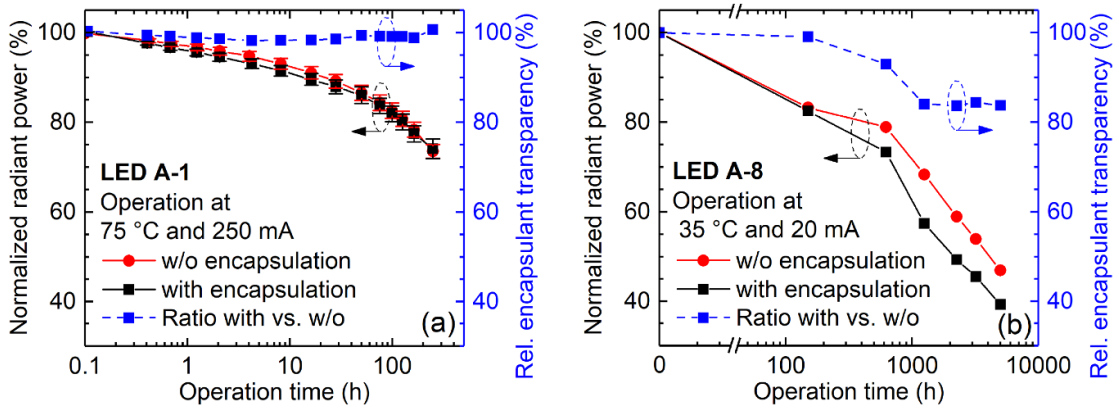

Figure 23. (a) Normalized radiant power of UVC LEDs A-1 (a) and A-8 (b) with and without encapsulation during operation. The LEDs A-1 were purchased in the year 2021 and were operated at a temperature of $T_{hs} \approx 75$ °C and an operating current of 250 mA. The LEDs A-1 were purchased in the year 2018 and were operated at a temperature of $T_{hs} \approx 35$ °C and an operating current of 20 mA. The relative encapsulation transparency was calculated by the ratio of the radiant power curves.

spectra of aged and unaged LEDs can sometimes differ significantly (figure 22). The contribution of parasitic emission can strongly increase at such low currents.

2.3. Degradation of UVC LED packages

To find out whether the encapsulation used in UVC LEDs degrades during operation, the standard encapsulation of LED A-1 was removed, and packaged LEDs with encapsulant (10 samples) and without encapsulant (4 samples) were operated for 250 h. The radiant power from these samples was averaged and plotted in figure 23(a). Within the error bars (standard deviation from the variation from sample to sample), no difference could be determined from the degradation curves. The relative encapsulation transparency (blue) is calculated by dividing the radiant power with encapsulation by the radiant power without encapsulation. It can be used as a measure to observe changes in the encapsulation. As the relative transparency remains stable at 100%, it could be concluded that the encapsulation of A-1 UVC LEDs did not degrade during the 250 hour operation. This is an example of a material that is suitable for operation under these conditions, at least within the first few hundred hours. The stability of this material over even longer periods of operation has not yet been investigated.

A comparable test was performed on an older generation LED (A-8) similar to sample A-1 (shown in figure 23(a)) with an organic encapsulant deposited over a smaller chip and designed for operation at a lower current of 20 mA. Figure 23(b) shows the relative radiant power for LED samples with and without organic encapsulant (after mechanical removal). It can be seen that the relative encapsulant transparency decreases after a few hundred hours and reaches a stabilized value of 84% after 1000 h operation.

One of the first types of UVC LED packages, which was manufactured in 2019 and is currently no longer in production, had an organic-based encapsulation layer over the UVC LED chip. Such a layer was intended

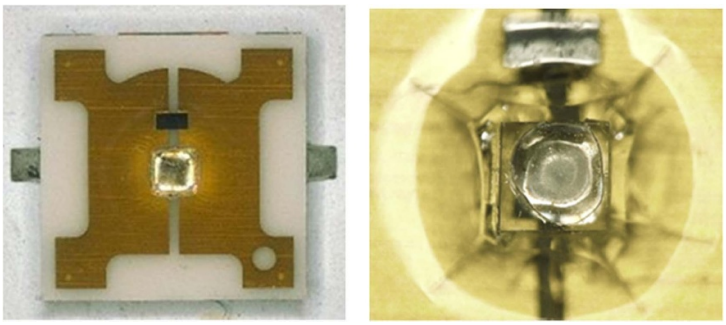

Figure 24. View of an early version of UVC LED (H-1) with an organic-based encapsulating layer before (left) and after (right, magnified) operation under 30 mA at $T_{hs} = 60\ ^{\circ}C$ for 300 h. The encapsulating layer was cracked after operation, causing significant loss in UVC radiant power.

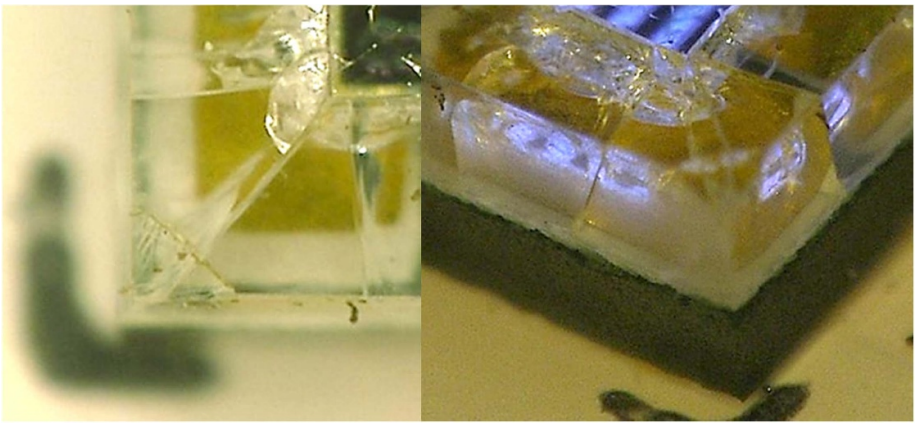

Figure 25. Top (left) and angled (right) magnified views of UVC LED C-7 with an organic-based encapsulating layer after operation under 20 mA $T_{hs} = 25\ ^{\circ}C$ for 7500 h. The encapsulating layer was cracked after operation, causing significant loss in UVC radiant power.

to increase the extraction of UVC radiation from the LED chip and serve as a protective layer against the environment. However, it was found that prolonged exposure (several hundred to several thousand hours) of this organic encapsulation layer to UVC light leads to severe degradation of the material during prolonged operation, resulting in significant deterioration of light transmission, curing and ultimately cracking. Cracks in the encapsulation layer can also lead to the LED chip being exposed to the environment and being damaged by the environment [6]. Furthermore, it can cause additional scattering and loss of UVC light within the LED package.

In their work, Lu *et al* compared the quartz glass and a silicone rubber as encapsulant for 280 nm UVC LEDs, demonstrating a higher initial intensity and a lower optical power degradation over time for the quartz glass-based samples [25]. A complete study on materials used as encapsulant for DUV devices was provided by Nagasawa and Hiranoin [26]; here, the author reviewed the long-term reliability of several polymers, pointing out the problematics related to the high-energy light exposition, the non-optimal refractive index, and the losses at the interface sapphire/resins caused by the differences in material affinity.

UVC LED H-1 is one example of such early package types with organic-based encapsulating layers that exhibited cracking (figure 24). The degradation of the encapsulation led to a halving (compared to the undamaged encapsulation) of the radiant power in the direction of the normal. Another example is UVC LED C-7 after 7500 h of operation (figure 25), where cracking reduced the radiant power at wide emission angles by ≈10%, whereas the radiant power in the direction of the normal remained almost unchanged. Such effects can therefore influence not only the absolute radiant power, but also the far field emission pattern (see also figure 1).

Adhesive organic-based resins are often used as an adhesive material to bond front quartz cover glass windows to the top of the cavity for ceramic-based UV LED packages (see figure 1, type (b)). If the process for adhesive dispensing is not well controlled, excessive adhesive residues can be present on the inner surface of the cover glass, partially covering the peripheral part of the surface. Figures 26(a) and (b) shows two examples of such adhesive residues. These layers are thin and reasonably transparent to UVC radiation and

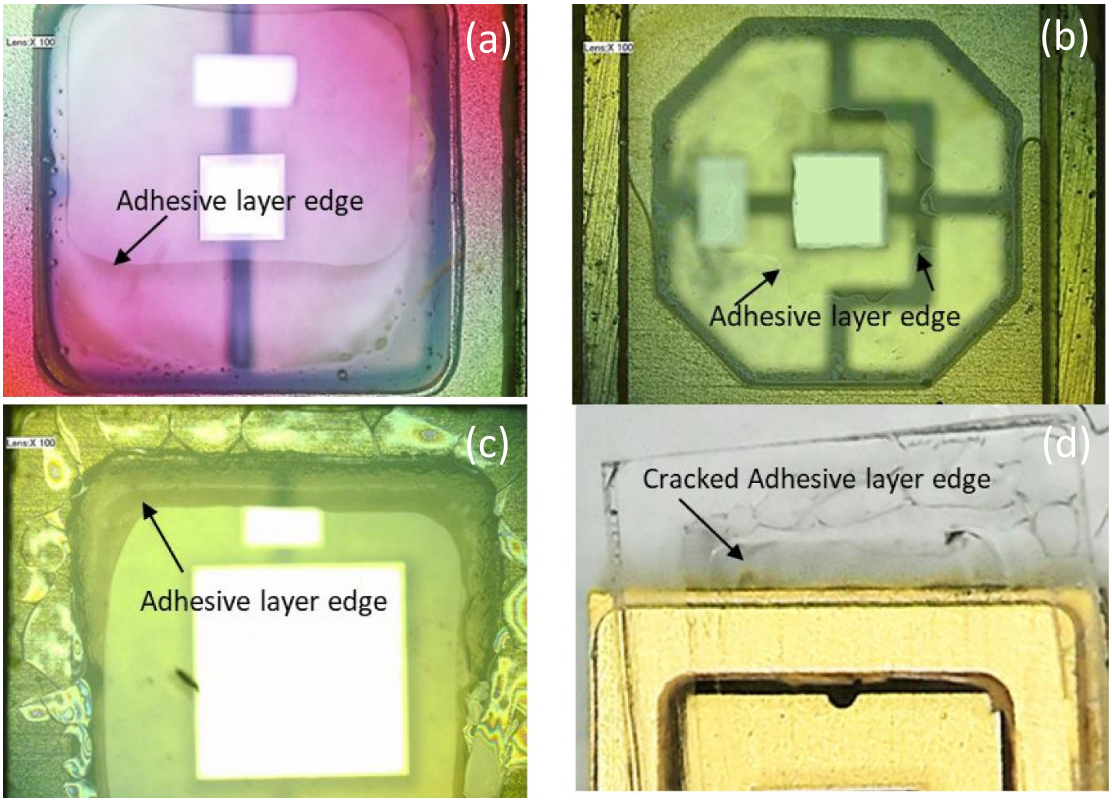

Figure 26. Examples of UVC LEDs with excessive adhesive residues on the front quartz cover window (a) and (b). View of cracked adhesive resin layer (c) causing complete detachment of quartz window (d) (from UVC LED E-2 after 3000 h operation at 350 mA and $T_{hs} = 30\ ^{\circ}C$).

might initially have minimal impact on total flux from UVC LED package. However, during LED operation, strong UVC irradiation will cause damage to this material, reducing its UV transmittance.

It was found that the adhesive properties of some organic-based adhesive resins for quartz cover glasses in UVC LED cavity packages deteriorate under strong UVC irradiation during prolonged LED operation. The material of the adhesive layer becomes harder, more brittle and shrinks in volume, which leads to cracks and delamination of the glass from the LED cavity package. This increases the probability that the LED chip is exposed to the environment. In some cases, quartz cover window can even detach completely from the UVC LED package. Figures 26(c) and (d) shows the formation of cracks in the adhesive layer and the complete detachment of the quartz window from the UVC LED E-2 after 3000 h operation. In addition, excessive thermo-mechanical stresses on the adhesive layer between the quartz glass and the ceramic cavity can also lead to detachment of the quartz window from a UVC LED package.

Packages for UV LEDs play an essential role in protecting the UV LED chip from environmental impact, especially from moisture and water vapor ingress during storage or during operation under excessive humidity conditions. There are UV LED hermetic package types on the market, where the quartz cover is soldered to the ceramic cavity. However, the majority of UVC LEDs are manufactured using more cost-effective gluing methods utilizing organic adhesives either in a few local spots or over the entire edge of the quartz cover cap. In most cases where such organic adhesives are used, the integrity of the packaging is not sufficient to prevent moisture permeability.

When water vapor is present in direct contact with the chip, it can cause moisture-induced corrosion of the epitaxial and contact layers. Figure 27 shows the evolution and propagation of moisture-induced corrosion of UVC LED chip F-1 at different times during high humidity and high temperature operation. The corresponding wet high-temperature operational life (WTHOL) stress conditions were: An operating current of $I = 20$ mA, a heat sink temperature of $T_{hs} = 65\ ^{\circ}C$, an ambient temperature of $T_a = 60\ ^{\circ}C$, a duty cycle of 50%, and a relative humidity of RH = 90%. Corrosion is initiated at one or few points at the edge of the chip mesa and propagates further over the entire n- and p-type regions of the UV LED chip. This process continues until LED chip operation is disrupted completely either as a short-circuit failure mode, or as an open circuit or high-resistive failure mode. Failure analyses using focused ion beam cross-sectioning and scanning electron microscopy with energy dispersive x-ray (SEM-EDX) revealed that aluminum-containing epitaxial layers were oxidized by a moisture-induced corrosion process. This process is similar in origin and

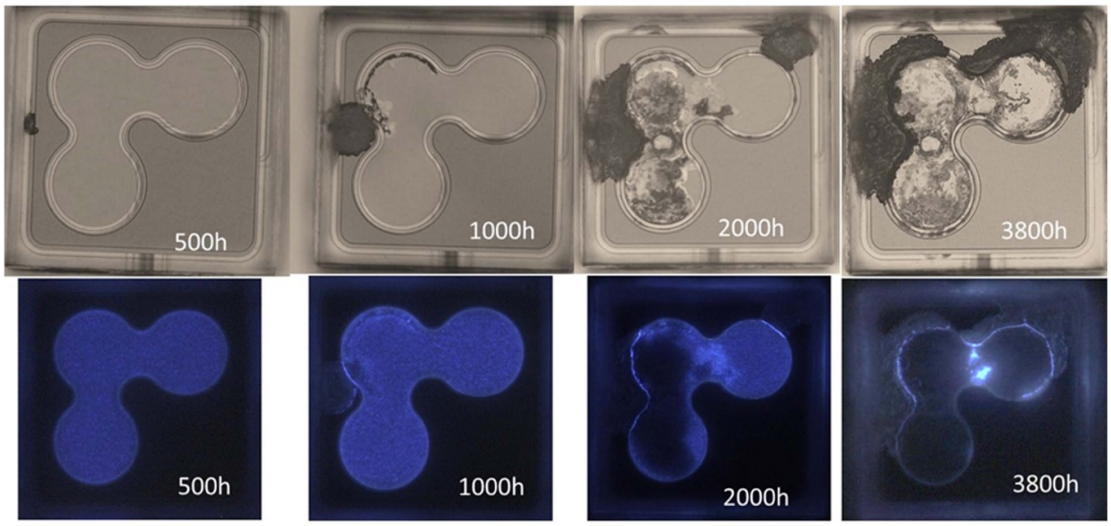

Figure 27. The evolution of moisture-induced corrosion in UVC LED chip F-1 in a light microscope at different times (upper row). The bottom row shows the corresponding spatially resolved electroluminescence emission. The LED was operated under wet high-temperature operational lifetime (WTHOL) stress conditions.

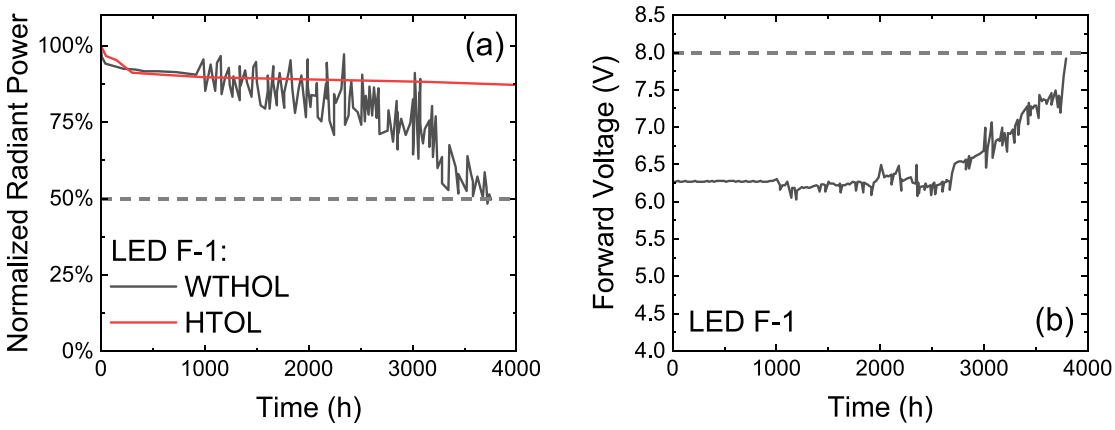

Figure 28. *In situ* changes in (a) normalized radiant power and (b) forward voltage during WHTOL (a) and (b) and HTOL (a) testing. UVB LEDs F-1 were used in these tests. Stress conditions for WHTOL and HTOL were: $I = 20$ mA, $T_{hs} = 65$ °C.

mechanism to other degradation processes that have been observed, for example, in visible high-voltage LED chips based on InGaN that are operated directly with alternating current (AC-LEDs) [27].

Figure 28 shows the *in-situ* changes in the normalized radiant power and forward voltage for UVC LED F-1 during WHTOL operation. The noisy progression of the WHTOL measurement curve can be associated with chip corrosion. The red line is the normalized radiant power graph (figure 28(a)) and corresponds to the stability trend for the same UVC LED subjected to the same conditions, but under dry ambient conditions HTOL. It can be seen that the radiant power decreases faster under the WTHOL test and the operating voltage also increases due to corrosion.

Figure 29 shows the changes in the current dependencies of the EQE (a), the radiant power (b), and the voltage (c) and (d) of the UVC LEDs F-1 under WHTOL conditions at different operation times. Here black corresponds to the initial LED before operation, red to the LED after 2000 h of operation with extensive degree of corrosion, and blue to the LED after 3800 h of operation. In the latter case, the degree of chip corrosion is severe, so that the electrical resistance increased drastically, and light is only emitted by small remaining areas (Compare with figure 27).

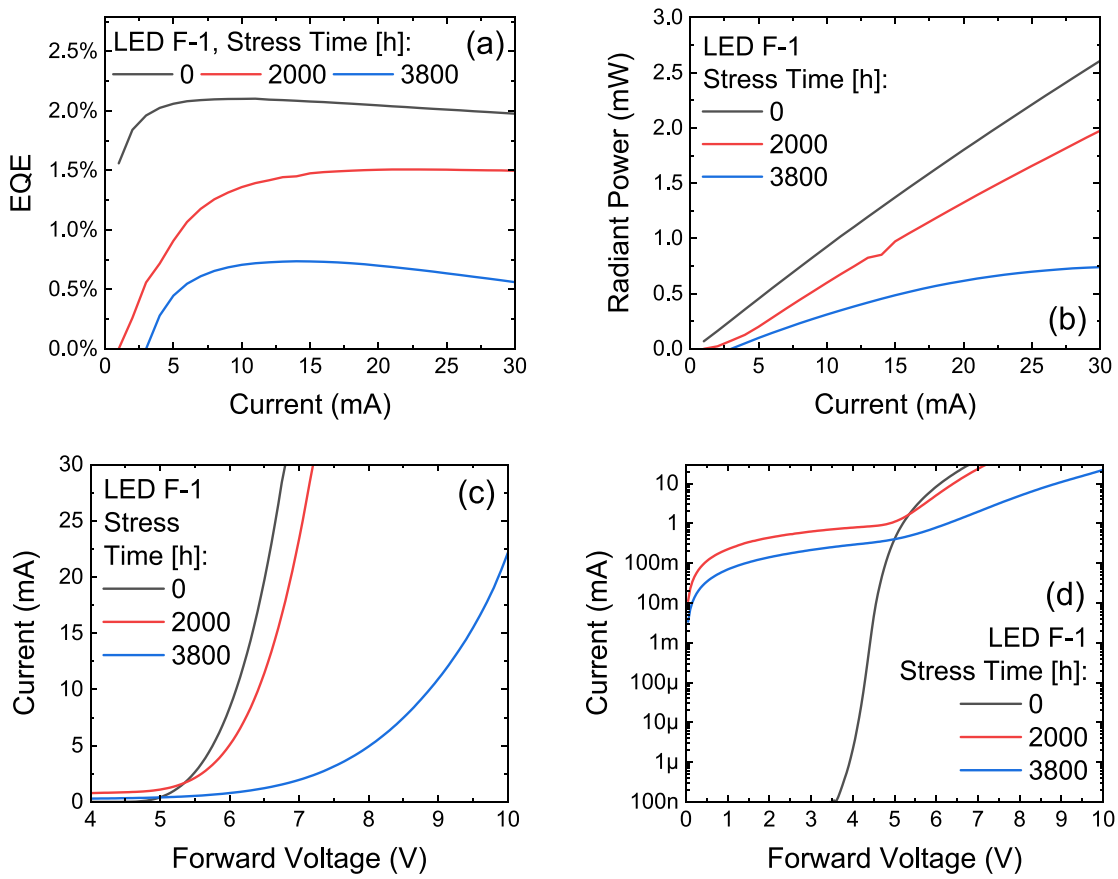

Figure 29. (a) Changes in linear current voltage plots. (b) Same current–voltage plot but on a logarithmic scale. (c) Change in the radiant power vs. current. (d) Change in the EQE vs. current. Results obtained during WHTOL testing. UVC F-1 LEDs were used in these tests.

3. Physical understanding of degradation—selected topics

3.1. Mathematical description of time dependencies of degradation effects

3.1.1. Gradual degradation

One of the goals of accelerated lifetime tests (ALTs) is to extract a mathematical model capable of describing the trend of a particular performance figure of the device during aging, to predict the parametric failure of the device according to a specific criterion, such as R70, R80, or R90 [28]. For visible solid-state emitters, a classical exponential function ($OP(t) \propto e^{-t/\tau}$) has been typically used to model the trend of the relative flux depreciation (including radiant flux) after the first 1000 h of operation [28, 29], however, recent works demonstrated that purely exponential decays do not represent the best mathematical description of the optical degradation kinetics related to UVC, UVB and UVA LEDs.

For instance, Ruschel *et al* [21] investigated the degradation behavior of 310 nm UVB LEDs stressed at various current densities (from 34 to 201 A cm^{-2}) in iso-thermal aging conditions (90 ± 5 °C), i.e. while maintaining the junction temperature T_j constant across the different experiments, to quantify the impact of solely the current density on device degradation. To fit the experimentally observed *OP* trends, referred to as $OP(t)$, the authors proposed a model described by the logarithmic formula in equation (3.1):

$$OP(t) = -\beta \cdot \ln\left(\alpha \cdot J^3 \cdot t + e^{-\frac{1}{\beta}}\right) \tag{3.1}$$

in which J represents the stress current density, whereas α and β are fitting parameters that were kept constant for all the investigated current levels. The results showed a correlation between the degradation mechanism and the cube of the imposed stress current density, suggesting that optical degradation was driven by a recombination-enhanced (RE) process [30] where three charged particles are involved, such as the Auger–Meitner recombination [31].

Another proposed model that considers the Auger–Meitner recombination as a possible driving force for optical degradation is the one suggested by Piva *et al* [32]. In this work, the authors hypothesize that the energy released by Auger–Meitner recombination events is sufficient to induce the de-hydrogenation of

gallium vacancies ($V_{Ga}H_n$), which could either re-bond with the released hydrogen ions or reach a stable de-hydrogenate state, if the hydrogen is removed. Calling A the initial state with the $V_{Ga}H_n$, B the state where the gallium vacancy is de-hydrogenate ($(V_{Ga}H_{n-1})^- + H^+$), and C the final state where the vacancy is de-hydrogenated and the hydrogen removed ($2(V_{Ga}H_{n-1})^- + H_2$), the authors proposed the following system of ordinary differential equations (ODEs) given in equation (3.2) to describe the optical degradation:

$$\begin{cases} \frac{dA(t)}{dt} = -k_{AB} \cdot A(t) + k_{BA} \cdot B(t) \\ \frac{dB(t)}{dt} = +k_{AB} \cdot A(t) - k_{BA} \cdot B(t) + k_{BC} \cdot B^2(t) \\ \frac{dC(t)}{dt} = +k_{BC} \cdot B^2(t) \end{cases} \tag{3.2}$$

Where the k_{ij} are the rate coefficients between the states, and they are used as fitting parameters. Here, the variation of $C(t)$, which represents the estimated variation of de-hydrogenated vacancies and so the increase in NRRCs, showed a good correlation with the overall variation in optical power during the aging considering $OP(t) \propto 1 - C(t)$..

Following up on the hypothesis of optical degradation assisted by Auger–Meitner recombination events, Piva *et al* in [32] compared a series of UVC LEDs with different Mg concentrations in the EBL, and they evaluated the optical degradation during a 330 h ALT at stress currents from 77 mA to 100 mA, depending on the Mg percentage in the EBL (see figure 30(a)). Starting from Hill's formula, which is typically used to describe the balance of chemical reactions involving the binding of ligands to macromolecules [33], the authors proposed the following function to describe the measured *OP* trends:

$$OP(t) = 1 - \frac{1-a}{1 + \frac{b}{(t+c)^d}}. \tag{3.3}$$

Here, a, b, c, and d are fitting parameters and they are kept constant for different curves, except for b, which is correlated to the Mg concentration in the EBL. The function supposes that the optical power is 1 for $t = 0$, and tends to a for $t \to \infty$. The decrease follows a logistic function, where the exponent d indicates the velocity to reach the final plateau value of the optical power.

A fourth possible equation proposed to fit the optical degradation of 275 nm UVC LEDs is reported by Zhang *et al* in [34], where the authors presented the formula shown in equation (3.4) that is based on the generation of NRRCs:

$$OP(t) = \frac{A_0 + H}{A_0 \cdot \ln(k \cdot e^{at} - k + e) + H}. \tag{3.4}$$

Here, A_0, H, k, and a are fitting parameters, where A_0 and H can be extrapolated from the initial LED EQE curve. This formula is developed for UVC LEDs aged up to 10 000 h at currents of 250 mA and 350 mA, and at room temperature (25 °C), it is deduced assuming that defect generation is the sole cause of IQE decay, and it occurs to maximize the entropy of the defects. The function supposes a logarithmic decrease in optical power with time, where the parameters A_0 and H are correlated with the concentration of NRRCs.

Figure 30(b) depicts a comparison of the results obtained by using the previously presented equations (3.1), (3.3) and (3.4) to fit the data reported in [21]. It can be seen that the equations proposed by the standard IES TM-21 [28] and by [34] cannot correctly replicate the experimental data. Instead, physics-based fitting formulas, mostly relying on the assumption of RE defect generation [32, 36, 37] seem to provide a good replica of the experimentally observed optical degradation trends.

Finally, it should be considered that since no strict correlation between the degradation of the radiant power and the variation in the electrical characteristics has been found so far, the related kinetics have not been fully investigated, yet. This leaves open questions and room for future studies focused on the investigation and the impact of degradation on the electrical and radiometric characteristics of the device.

3.1.2. CFs

As already shown in section 2.2, CF can occur during the operation of LEDs. A CF event of a single LED typically occurs suddenly and unpredictably. Nevertheless, the statistical frequency of such a failure can be described mathematically. However, this requires a sufficiently large number of LEDs for which a CF event occurs. A sufficiently large number of CF events is depicted for a batch of UVB LEDs in which such failures occurred more frequently due to a non-optimized chip design (red squares in figure 31). In this case, a total number of 270 UVB LEDs were operated for 1000 h. The LEDs were operated at a current of 100 mA (67 A cm^{-2}) and a T_{hs} value of 20 °C. The number of CF events was cumulated, and the percentage of CF events was plotted over time. As shown for the red squares the temporal progression of the proportion of CF

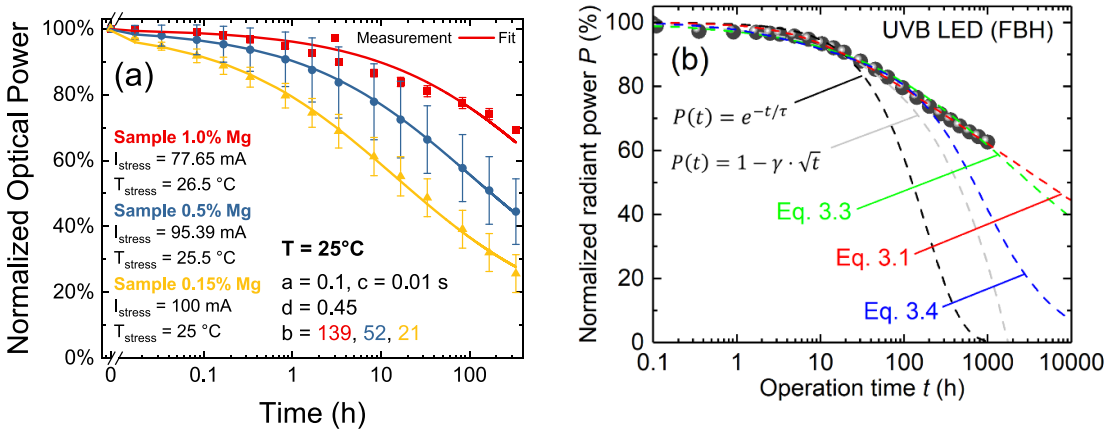

Figure 30. (a) Fitting of the data with the formula proposed in. Reproduced from [35]. CC BY 4.0. (b) Comparison of the different formulas proposed to fit the relative optical power degradation on the data presented in [21].

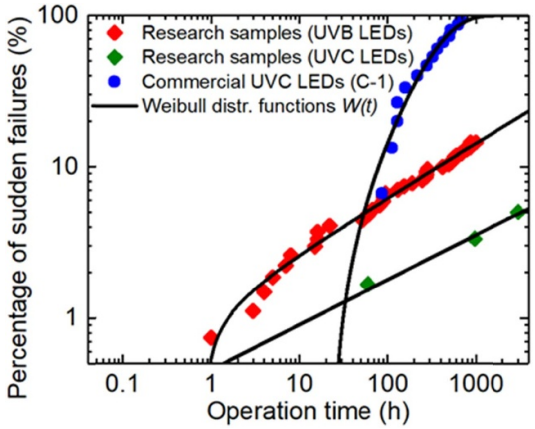

Figure 31. Percentage number of catastrophic failures during long-term operation of 270 samples of UVB LEDs (red), 60 samples of UVC LEDs (green), and 15 samples of commercial UVC LEDs from manufacturer C (blue).

Table 2. Parameters of the Weibull distribution function fits in figure 5.

Exemplary LED samples	k	T (h)	$t0$ (h)
Research samples (UVB LEDs)	0.38	1.4×10^5	1
Research samples (UVC LEDs)	0.30	6.5×10^7	0
Commercial UVC LEDs (C-1)	1.22	376	23

events can be approximated using a Weibull distribution function $W(t)$ of the form:

$$W(t) = 1 - e^{\left(\frac{t-t_0}{T-t_0}\right)^k}. \tag{3.5}$$

Where T is the characteristic time that can be interpreted as operation time after which CF's occurred in all devices. The parameter $t0$ is the threshold time in which CFs are highly unlikely, and k is the shape parameter. Values $k < 1$ indicate that the failure rate decreases over time, values $k = 1$ indicate that the failure rate is constant over time and values $k > 1$ indicate that the failure rate increases over time. For the example above, the Weibull parameters are listed in the table 2.

This function cannot be used to predict the failure of an individual LED. However, such a Weibull function indicates the frequency of occurrence to be expected for a certain operation time. Also shown is the example of 60 UVC LEDs in long-term operation (with on/off cycles of 5 min/5 min) at 200 mA (50 A cm^{-2}) and T_{hs} value of 20 °C, at which the probability of CF events is significantly lower (Green squares in figure 31). There is an indication that the three detected CF events follow the Weibull distribution shown. However, as the probability of CFs is significantly lower, the number of LEDs tested is too small or the

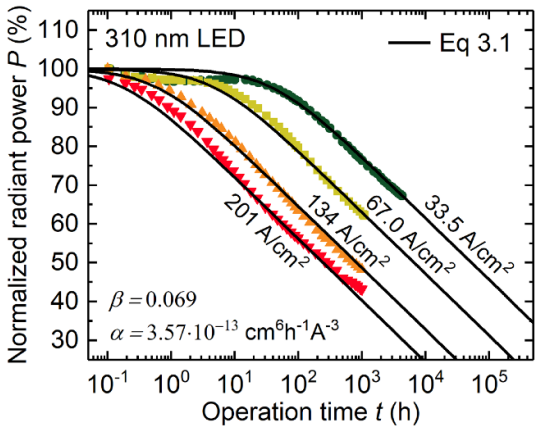

Figure 32. Normalized optical power of UVB LEDs operated at different nominal current densities versus the logarithmic time scale. Reproduced with permission from [21].

operation time too short to provide statistical certainty. The associated Weibull parameters determined from the fit are therefore highly inaccurate.

Furthermore, the temporal distribution of CF events of 15 LEDs from manufacturer C (blue circles) is shown, since many such failures were detected in these samples during the test period (see also section 2.2). Here the LEDs were operated at a continuous current of 350 mA as recommended in the data sheet and at a temperature of $T_{hs} \approx 25$ °C. Due to the high probability of CFs, the relatively small number of LEDs tested is already sufficient to be described by equation (3.5). For the other manufacturers examined, however, the number of detected CF's was too low to be depicted and described by equation (3.5).

3.2. Degradation effects of LED chip

3.2.1. Acceleration factors—current density (or carrier density), temperature, Auger–Meitner recombination

The impact of the nominal current density on the degradation of UVB LEDs with peak emission wavelength at 310 nm was studied previously [21]. Here, the nominal current density is defined as the current divided by the area of the active region, assuming a laterally homogeneous current injection. The investigated UVB LEDs were operated at different current densities between 33 A cm^{-2} and 201 A cm^{-2}. To separate the impact of current density from that of the temperature, the junction temperature was kept constant at ≈90 °C by adjusting T_{hs} for each applied current. A similar experiment was carried out on UVC LEDs with a peak emission wavelength at 265 nm. Here, the current density was varied between 30 and 120 A cm^{-2}, which corresponds to operating currents between 100 and 400 mA. Furthermore, to be able to compare the degradation state of the LEDs stressed under different operation conditions, the optical power was measured under the same comparable conditions during long-term operation. This is particularly important here because the relative power change can typically be different for different measurement currents, which can be recognized by the increasing non-linearity of the *P–I* curves (compare figure 17 in section 2.2.4). Only the power measured under the same measurement conditions during operational stress test at different stress currents (or current densities) enables the effect of the acceleration of degradation by the current density not to be superimposed by the effect of the increase in the non-linearity of the *P–I* characteristic curve.

For this purpose, the respective long-term experiments were interrupted several times at specific points in time in order to measure the optical power of all LEDs at a temperature of $T_{hs} \approx 20$ °C and a nominal measurement current density of ≈30 A cm^{-2}. The results are shown exemplarily for the UVB LEDs in figure 32. It turned out that the current density is a strong acceleration factor for the degradation of the optical power. The data could be well described with the logarithmic function (equation (3.1)) indicated by the black solid lines. Accordingly, the R70 lifetime (*t70%*) scales inversely with the nominal current density as shown in equation (3.6):

$$t_{70\%} \propto \frac{1}{j^{\gamma}}, \tag{3.6}$$

where the exponent is $\gamma \approx 3$. A similar result was also obtained for the investigated UVC LEDs, resulting in the depiction in figure 33, where the normalized radiant power is plotted versus the operation time multiplied with the cube of the nominal current density. The fact that the curves lie on top of each other suggests that there must be a current-driven degradation mechanism that takes place in the same way in UVB

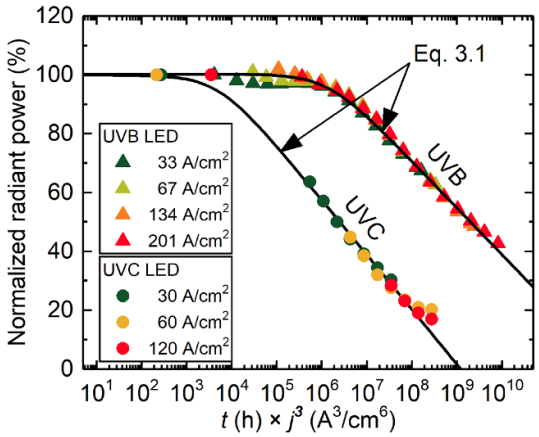

Figure 33. Normalized optical power of UVB and UVC LEDs (research samples) versus the product of operation time t and cube of the nominal current density j.

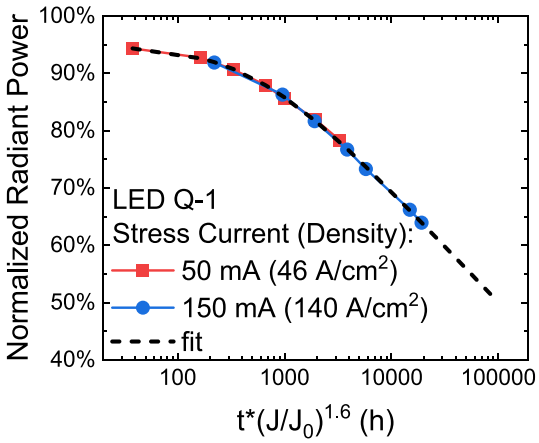

Figure 34. An alternative plot for UVC LEDs lifetime results @50 mA (blue line) and 150 mA (red line) and fit (black dashed line) with equation similar to equation (3.1), with a time axis scaled with the current density $(J/J_0)^{1.6}$, where J is the stress current density and J_0 is the reference current density (≈93 A cm^{-2} @typical binning current of 100 mA).

and UVC LEDs. However, the current density dependency of the R70 lifetime certainly depends on several factors such as the homogeneity of the current distribution (see figure 43), but also on the charge carrier distribution in the active region. The exponent γ can therefore deviate and can be smaller or larger than $\gamma \approx 3$. In general, the observations are in line with previous reports on InGaN-based LEDs. Evidence for current-dependent degradation rates could be found both on high-power white LEDs [38] and on blue-violet LEDs [39]. The degradation was found to be triggered at high recombination rates, thanks to the execution of stress experiments under optical excitation [40].

It is worth mentioning that—for many applications—only the change in radiant power measured under operating conditions is relevant. It must therefore be considered here that the exponent is typically $\gamma \leqslant 3$ if the measurement of radiant power over time is carried out under the same conditions as long-term operation. In this case, the degradation dynamics are superimposed by the increasing non-linearity of the *P–I* characteristic at low currents. This means that even if the degradation process is significantly slower at low currents, the relative change in power can be greater at low measurement currents due to the non-linearity. This effect is shown as an example in figure 34, where the radiant power was measured at the same conditions as stress current used in long-term operation. This results in an exponent of around $\gamma \approx 1.6$, and such power factor value is comparable to power factor value of 1.5 for lifetime dependence versus stress current suggested in [34].

Since the charge carrier density in the active region is directly influenced by the current density, it was assumed that a recombination-driven process must be responsible for the current-induced degradation. Due to the comparatively large exponent $\gamma \approx 3$ of the current density dependence, it was concluded that the driving mechanism could be Auger–Meitner recombination which is a three-particle process. Therefore, its

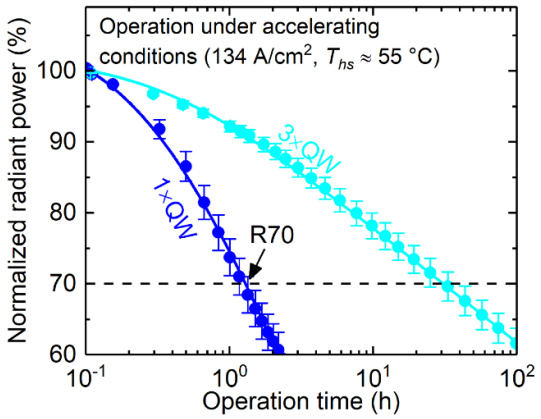

Figure 35. Normalized radiant power of UVB LEDs with a single and triple QW active region operated at the same nominal current density of 134 A cm2 at $T_{hs} \approx 55$ °C.

rate has a stronger dependence on the charge carrier density than, for example, the rate of radiative recombination or SRH recombination.

However, this also means that the degradation rate strongly scales with the charge carrier density in the active region. This conclusion was confirmed by an experiment in which the number of QWs in the active region of a UVB LED was varied [41]. Here, the measured radiant power of the LED with a single QW was about 30% higher than that of the reference LED with three QWs. Therefore, assuming that each QW contributes equally to the emitted radiant power, the density of the overlapping charge carriers in each of the three QWs must be at least three times lower on average compared to the single QW LED. This was also confirmed by a simulation of the carrier density distribution. Accordingly, the Auger–Meitner rate in the quantum wells of the reference LED should be significantly lower and the reference LED should have a significantly lower degradation rate. In fact, long-term operation at the same nominal current density showed that the reference LEDs have an R70 lifetime that is approximately 20 times longer than that of the single QW LEDs (figure 35). This large difference in lifetime supports the hypothesis that Auger–Meitner recombinations are involved and that the degradation rate scales with the carrier density in the active region. In addition to Auger–Meitner recombinations, radiative recombinations also become more likely with increasing overlapping charge carrier densities. It is therefore to be expected that an increase in the emission power of an LED can generally be accompanied by an acceleration of degradation. The hypothesis could thus explain the observed negative correlation (figure 10) between R90 lifetime and radiant power.

As the results in section 2 have already shown, besides the current density, the temperature can be a strong acceleration factor for the radiant power degradation of UVC LEDs as well. The fact that the operation of UVC LEDs at elevated temperatures can lead to a more rapid reduction in the radiant power has also been observed in research samples (see type 1 in figure 36). For example, Gong *et al* observed that the degradation rate in AlGaN-based UVC LEDs increases strongly with the operating temperature [42]. An activation energy of 0.27 eV could be determined by means of an Arrhenius plot. Furthermore, Meneghini *et al* [43] found a similar behavior in GaN-based LEDs emitting in the visible spectrum. The authors exposed the LEDs to stress at temperatures of up to 250 °C and calculated an activation energy of 1.3 eV. The temperature dependence was associated with the hydrogen contained in the insulator, which interacts with the acceptor dopants in the p-side.

The results suggest that there are temperature-driven mechanisms (e.g. diffusion processes) which, in addition to the current density, lead to degradation of the device during operation. Nevertheless, a different behavior has already been observed in research samples (see type 2 in figure 36). In this case, an increased operating temperature does not appear to contribute to an acceleration of degradation. In some cases, radiant power of UVC LEDs has even been observed to reduce more slowly during operation at elevated temperatures. The results indicate that temperature-driven degradation mechanisms, which are often observed in commercial LEDs, do not necessarily occur in every UVC LED. It can therefore be assumed that there is a parameter in the semiconductor layer design that can be used to eliminate or at least minimize the effect of the temperature-driven mechanisms. However, more research is needed here, as the reasons for the temperature-dependent degradation are not yet fully understood.

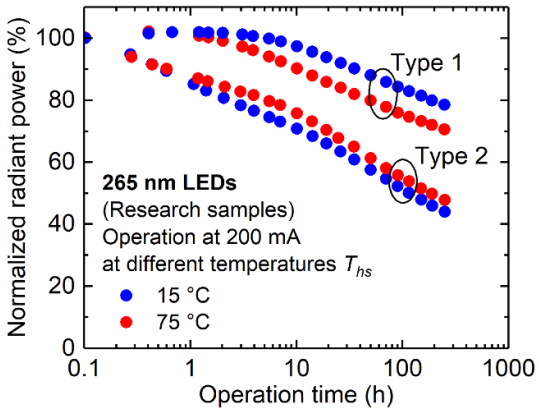

Figure 36. Normalized radiant power of UVC LEDs (Research samples) during operation at a constant current of 200 mA. The LED types were operated at different temperatures T_{hs} and showed a different temperature dependency.

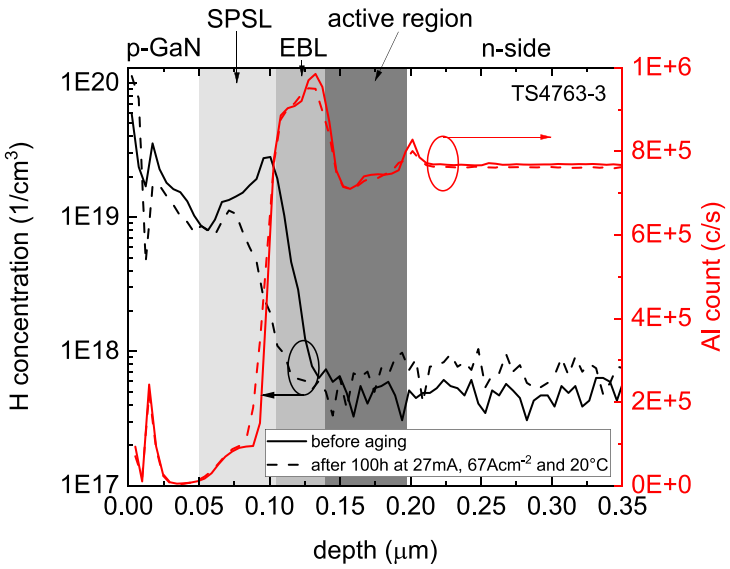

Figure 37. SIMS profile of a 265 nm LED measured before and after a constant current stress test of 100 h at 67 A cm^{-2}.

3.2.2. Current picture on the physical background of changes in the LED

Recent studies focused on the hypothesis that diffusion of hydrogen (H) through the LED structure is one of the driving forces responsible for the degradation of UVC LEDs.

The relocation of H atoms in the proximity of p-doped AlGaN layers during prolonged stress has been observed several times in literature. For instance, figure 37 reports the results of secondary ion mass spectrometry (SIMS) measurements carried out on 265 nm LEDs submitted to constant-current stress at 67 A cm^{-2} for 100 h. Compared to a not stressed device, a strong decrease in the concentration of H can be observed within the EBL and the interlayer (IL), indicating that the aging procedure induced the migration of the hydrogen. Chichibu *et al* reported the SIMS profiles of magnesium (Mg) and H concentration in 275 nm UVC LEDs at the beginning and at the end of a 300 h accelerated lifetime stress test [44]. The results confirmed that while the Mg profile does not show a change after stress, H exhibits a noticeable diffusion towards the n-side. The authors state that this redistribution could be caused both by the absorption of the highly energetic emitted UV photons (at 275 nm, the photon energy [E_{ph}] ≈ 4.51 eV) and by the Auger–Meitner recombination events, since both processes can provide sufficient energy to break Mg–H bonds (2.03 eV) and N–H bonds (4.05 eV) [44–46]. Once this happens, the newly formed point defects can act as NRRCs or charged centers [47], possibly resulting in a lowering of the overall radiant efficiency of the device. The authors investigated the physical origin of such defects by combining positron annihilation spectroscopy and time-resolved photoluminescence (PL) and ascribed them to vacancy complexes of V_{Ga} and V_N ($[V_{Ga}V_N]$) that could be passivized by $H^{0/+}$.

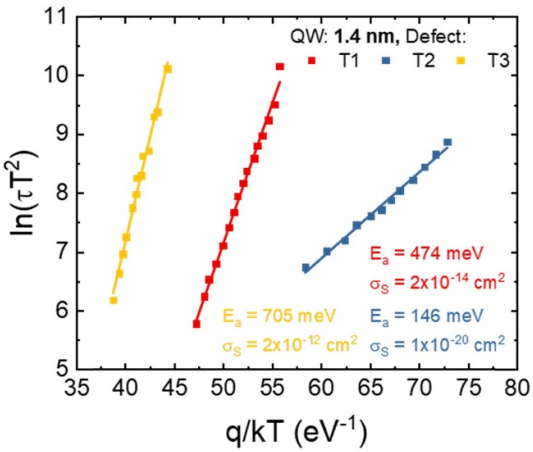

Figure 38. Arrhenius plot extracted from C-DLTS measurements during the aging procedure on a SQW 265 nm UV LED. Reproduced from [53]. CC BY 4.0.

The role of vacancy de-hydrogenation in the optical degradation of UV LEDs was also previously investigated [32]. In this work, the authors consider the de-hydrogenation of Ga vacancies, described by the reaction in equation (3.7):

$$V_{Ga}H_n \rightleftharpoons (V_{Ga}H_{n-1})^- + H^+ \tag{3.7}$$

as a possible mechanism favoring the increase in concentration of acceptor levels in the active region. This increase is supposed to lead to a modification in the band bending near the quantum wells, which ultimately reduces the injection efficiency in the active region. Additionally, once the vacancy is de-hydrogenated, the released H^+ ion can either re-bond with the vacancy, or it can bond with another hydrogen ion (and two electrons) to form molecular hydrogen (H_2). By describing these processes as a three-state system, the authors managed to model the optical degradation during the aging of the device with the system of ODEs reported in equation (3.2).

The idea of a correlation between optical power reduction and the de-hydrogenation of gallium vacancies was further refined by Roccato *et al* [35, 48], in which the authors revisited the balance model of the chemical species by leveraging Hill's formula [33], and obtaining the radiant power decay trend reported in equation (3.3). This model was then successfully applied to extract the characteristic R90, R80 and R70 lifetimes exhibited by certain commercial UVC LEDs submitted to accelerated stress tests [24].

Considering the solid evidence of the generation and the relocation of certain defects in the structure, it is possible to analyze their impact during LED operation. In wide bandgap devices, defects characterization can be achieved through the combination of non-invasive techniques such as capacitance deep-level transient spectroscopy (C-DLTS), deep-level optical spectroscopy (DLOS), photocurrent spectroscopy, and PL measurements [49–51]. In some cases, characteristic signatures of the defects, such as the Arrhenius plot associated to their emission process, can be extracted from the measurements and compared with other reports or databases available in literature (for instance, see [49] or [52] for C-DLTS on GaN).

As an example, Piva *et al* submitted a 265 nm research-grade UVC LED to a constant current stress for 200 h, which was regularly interrupted to carry out a C-DLTS characterization [53]. These measurements showed the presence of two traps related to Mg, also detected on the untreated device, and one trap associated with point defects of unknown origin that were generated during the stress test. As shown in figure 38, the authors found that trap T1 has an activation energy of 474 meV, and the authors associated its origin to Mg-related defects detected in n-type material, according to the hypothesis of back diffusion of Mg atoms towards the n-side during growth [54]. Trap T2 has an activation energy of 146 meV, and it could be ascribed to substitutional Mg acting as dopant located within p-GaN [55, 56], either at the p-side of the device close to the EBL or in correspondence with the partially rectifying p-contact. Finally, trap T3 has an activation energy of 705 meV, it is ascribed to point defects [57], and its concentration increases during the aging procedure, indicating the stress induced the generation or propagation of such type of defect within the epitaxial structure.

Hypotheses on the physical origin of defect generation were discussed by Ruschel *et al* in [21]. The Authors suggested a possible correlation between the increase in defectiveness and the rate of Auger–Meitner recombination events [21]. As already explained in section 3.1.1, the proposed model considers that the energy released by Auger–Meitner recombination events occurring during operation can promote the

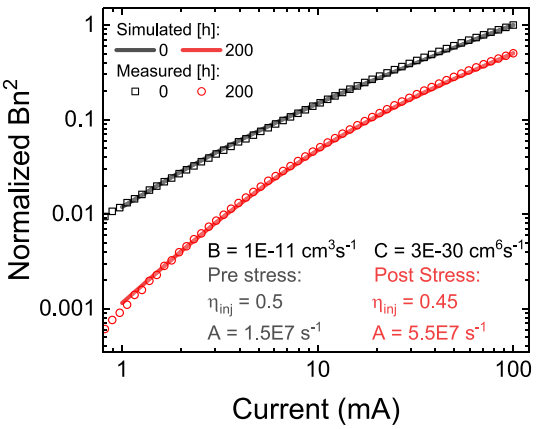

Figure 39. Normalized optical power before and after the aging procedure on a single QW 265 nm UV LED simulated starting from the classical rate equation. Reproduced from [53]. CC BY 4.0.

generation/activation of pre-existing point defects or complexes in proximity of the active region, ultimately inducing an increase in the rate of SRH recombination. The authors also suggest $V_{Ga}H_n$ complexes as a possible physical origin of the NRRCs activated by the Auger–Meitner events, in addition to $V_{Ga}V_N$ divacancy complexes, which become electrically active after the stress-induced removal of previously bonded hydrogen atoms. Finally, alongside the Auger–Meitner events, the high-energy UV photons emitted from the active region may also contribute to the generation of defects within the active region [44].

As mentioned above (section 3.1.1), defect generation can also lead to a variation in the electrical and optical characteristics of the devices, such as the increase in trap-assisted tunneling (TAT) related forward leakage current and the decrease in radiant power at low current levels detected in [32]. By means of DLOS, the authors of this work identified the presence of two deep levels, with activation energies of 1.6 eV and 2.15 eV in an energy gap of 4.35 eV, where the second turned out to be a very good candidate in contributing to TAT leakage current in the 2–3.5 V bias region, according to the results of the investigation reported in [58]. An increase in the concentration of such levels, experimentally observed through steady-state photo-capacitance measurements, was therefore found to be strongly correlated with the increase in the sub-turn-on conduction induced by aging. Additionally, the authors in [58] showed a good correlation between the concentration of the 2.15 eV defect with the decrease in optical power after 1000 min of aging, confirming the NRRCs nature of this trap.

Defect generation could affect also the carrier injection in the active region., Piva *et al* modeled the optical characteristics during a constant current stress test starting from the conventional rate equation given in equation (3.8) [53]:

$$\frac{\mathrm{d}n}{\mathrm{d}t} = \eta_{\mathrm{inj}} \cdot \frac{I}{qV} - An - Bn^2 - Cn^3 \tag{3.8}$$

where η_{inj} is the injection efficiency, V is the active region volume and A, B, and C are the coefficients for SRH, bimolecular, and Auger–Meitner processes, respectively. After tuning these parameters to fit the *L–I* characteristic at 0 h (see figure 39), while also being in compliance with values commonly reported in literature, the authors demonstrated that the sole increase in the A coefficient, or decrease in injection efficiency, is not sufficient to explain the current dependency of the observed variation in the *L–I* characteristics. On the other hand, a combined variation of these two parameters allowed to correctly match the *L–I* curve after the stress, thus indicating that both mechanisms occur at the same time during aging. To explain this behavior, the authors hypothesize that the defects generated in the active region could act simultaneously as NRRC and as charged centers impeding the injection of holes into the QW. This hypothesis was also supported by technology computer aided design (TCAD) simulations, which demonstrated how an accumulation of charge at the edge of the QW could significantly increase the potential barrier seen by the holes that have to be injected [53].

Similar conclusions are derived by Chichibu *et al* in [44], where the initial reduction in radiant power exhibited by 275 nm LEDs was associated with the decrease in injection efficiency caused by the activation of some shunt recombination paths originated from the depassivation of NRRCs at the p-side of the active region, i.e. in the p-doped EBL or in the p-AlGaN layer [44].

The aging-induced increase in defect concentration can also impact the electrical characteristics of the devices. As already reported [48], the electrical characteristics were modeled for a UVC LED with single QW

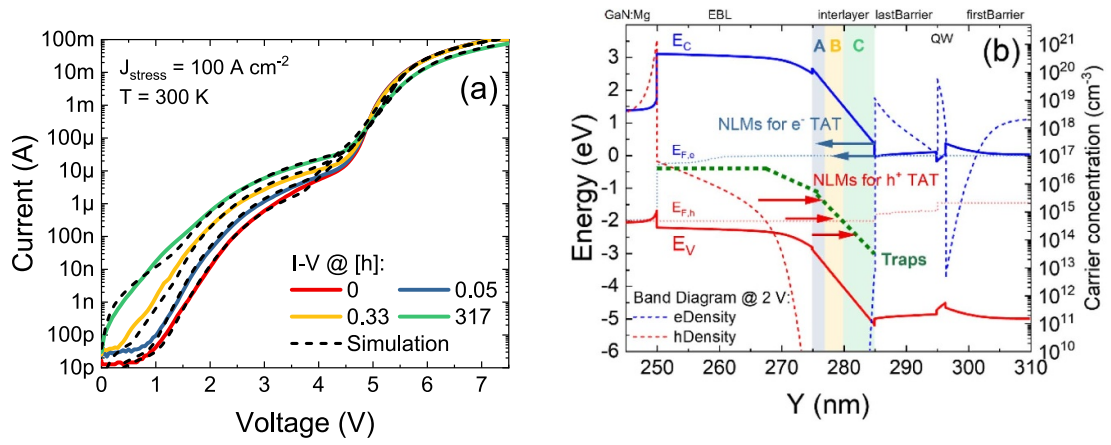

Figure 40. (a) Electrical characteristics during the aging procedure at 100 A cm^{-2} and room temperature (300 K), modeled with TCAD simulations. (b) Simulated band diagram of the structure in forward bias. Reproduced from [48]. CC BY 4.0. TAT stands for trap-assisted tunneling, whereas NLMs indicate the regions covered by the so-called 'non-local meshes', which for the adopted simulator correspond to regions where the TAT process is simulated.

(research sample), which was subjected to a constant current stress at 100 A cm^{-2} and at room temperature (25 °C) for about 300 h. The increase in leakage current below the turn-on voltage (figure 40(a)) is again associated with the generation of defects within the space-charge region, as demonstrated by the DLOS measurement. The authors used the experimentally determined defects properties as input parameters for their TCAD simulations. In particular, they subdivided the interlayer, grown between the top barrier and the EBL, into three regions, named A, B and C, as shown in figure 40(b). By tuning the defect concentration in each layer they were able (i) to reproduce the experimental *I–V* curve of the unaged device, and (ii) to demonstrate that the aging process was inducing a monotonic increase in the density of deep levels in device layers closer to the p-side, which is consistent with a defect migration process occurring from region A towards C [48].

Another effect of aging on the electrical characteristics of UVC LEDs is represented by the increase in the drive voltage of the devices. In the case study reported in [53], the authors ascribed this phenomenon to the worsening of the p-contact, caused by the passivation of Mg atoms near the p-GaN/metal interface. Aided by TCAD simulations, the authors showed that by slightly reducing the effective p-doping concentration within the first 20 nm of p-GaN close to the contact, it was possible to accurately fit the variation exhibited by the *I–V* characteristics during the stress.

The aging procedure also influences the ABC parameters of the conventional rate equation (3.8) typically employed to model the EQE vs. current characteristic of an LED. Neglecting the impact of photon extraction efficiency and injection efficiency, the EQE is directly proportional to the IQE (η_{IQE}), which is defined as the rate of radiative recombination over the overall recombination rate within the active region of the device, i.e. its QWs [11]. Considering this, an increase in the defectiveness of the QW can be directly mirrored into an increase in the *A* coefficient, and therefore in the rate of non-radiative SRH recombination events occurring per unit of time and volume within the active region of the device, defined by the *An* product. Starting from the model of Piva *et al* [53], using values for *A*, *B* and *C* similar to the ones reported in [59], and considering the increase in the *A* coefficient as the sole effect of a specific aging procedure, the EQE variation should follow the theoretical trend represented in figure 41(a). Here, it is possible to observe that an increase in *A* implies a reduction of the EQE peak and its shift toward higher current densities. The experimental EQE curves are calculated from the data reported in figure 39 at 0 h of stress.

The decrease in the overall rate of radiative recombination can also be caused by the decrease in injection efficiency. This can happen due to the formation of potential barriers in the structure that hinder the injection of carriers into the active region [53, 60]. Figure 41(b) reports the mathematical simulations of the variation in injection efficiency of a UVC LED: with respect to the variation in *A*, the injection efficiency has the greatest effect on the decrease of the EQE peak and rather less on the current density value at which the maximum is reached.

Another important process that could affect the optical characteristics of a UVC LED is the so-called thermal droop, i.e. the decrease in radiant efficiency at higher operating temperatures, and its variation during device aging. The common causes of thermal droop in UVC LEDs are: carrier overflow, carrier escape from quantum wells, trap-assisted escape, and trap-assisted leakage through mid-gap states [61]. Carrier

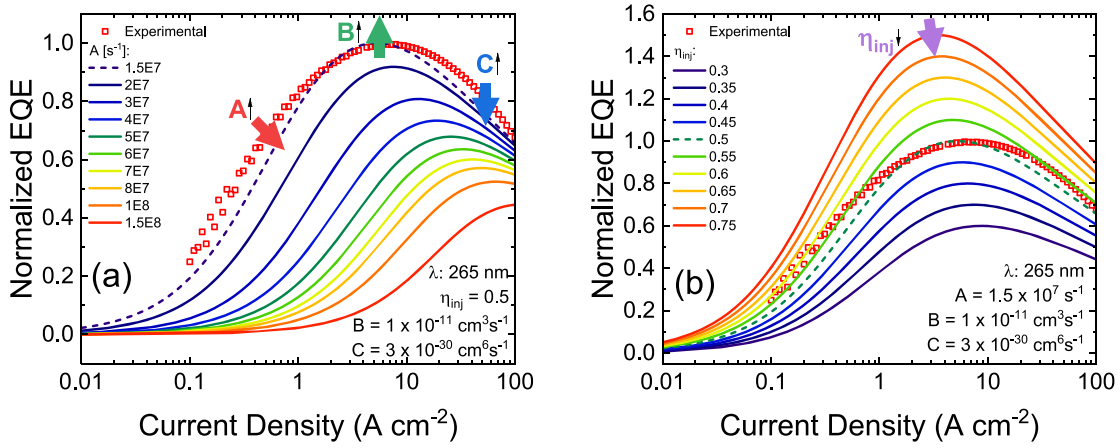

Figure 41. Mathematical simulation of the EQE of a single QW LED in function of (a) the A coefficient, and (b) the injection efficiency. All the curves are normalized at the EQE peak of the curve that best fits the experimental measurement (dash line).

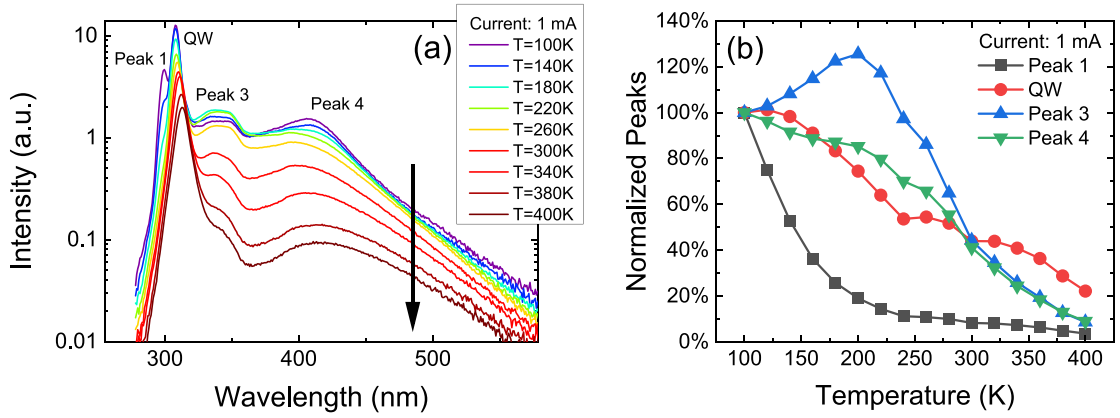

Figure 42. (a) Electroluminescence spectra of a UVB LED measured at 1 mA at various temperatures [17]. (b) Normalized peaks intensities as function of temperature. Reproduced with permission from [17].

escape and carrier overflow are strongly related to the conduction and/or valence band discontinuity between the QW and the barrier height. For typical UVC emitters, this value is small, due to the relative concentration of aluminum that needs to be employed to grow AlGaN-based active regions compatible with the emission of photons with energy >4.7 eV, (Al content is above 48% in the QWs of UVC LEDs emitting at 265 nm [61]). Trap-assisted leakage and trap-assisted escape are also both described by temperature-activated processes [62], which imply a reduction in the concentration of carriers in the active region with increasing temperature, ultimately leading to a decrease in the overall rate of radiative recombination.

Concerning the thermal droop analysis, De Santi *et al* performed an extensive study that analyzed the EL spectra of a 308 nm UVB LED in a wide range of temperatures (figure 42(a)) [17]. The trend of the emission intensity of the QW peak, reported in figure 42(b), could be divided into three operating scenarios: (i) at low temperatures (below 250 K) and low bias (below 1 mA), (ii) at low temperatures and high bias levels, and (iii) at high temperatures (above 250 K). In region (i) the optical power decrease follows the Arrhenius law, suggesting that the thermal droop is caused by the exciton delocalization, i.e. the temperature lowers the probability of an electron–hole interaction, decreasing the radiative recombination rate [63]. In region (ii) the EL intensity increases with temperature, indicating an improvement in the hole injection efficiency into the QWs. In region (iii), the radiant power decreases with temperature due to SRH recombination caused by deep levels, as confirmed by the model that the authors developed starting from the classical ABC rate equation.

Consequences of the aging on thermal droop can be found in section 2.1.2 and especially in [64], where the authors report a stronger stress-induced decrease in optical emission at higher operating temperatures, indicating the possible role of SRH recombination. Another effect that can negatively impact thermal droop could be the decrease in injection efficiency: carriers may require higher temperatures to overcome potential barriers located within the epitaxial structure if their height increases over stress [53], thus implying an

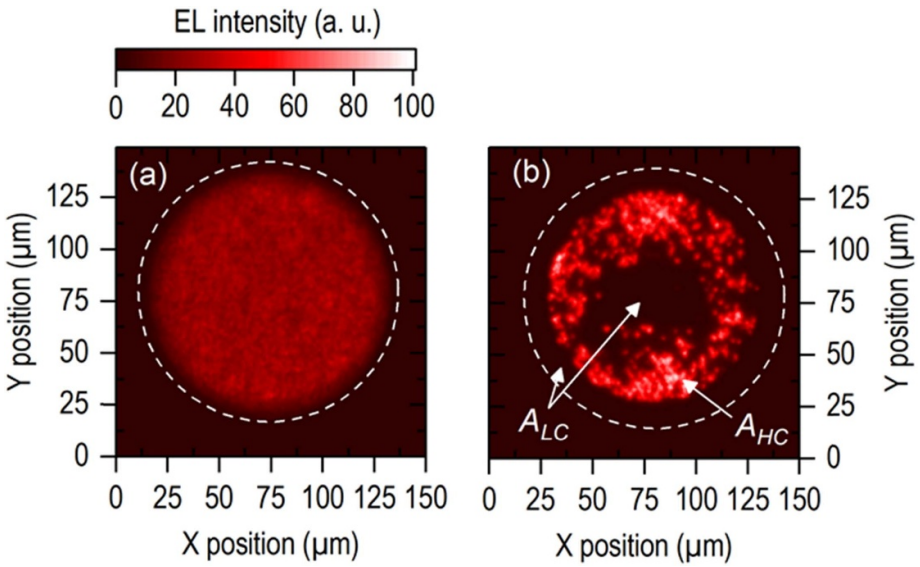

Figure 43. EL intensity image of a UVB LED (a) before and (b) after an aging test of 42 h at 200 A cm^{-2} at 29 °C. The distribution can be interpreted in a first approximation as the distribution of the current density. Reproduced with permission from [66].

increase in the dependency of optical efficiency of temperature, especially at low operating currents. The spectral purity and the thermal droop influence on 265 nm LEDs were studied by Ishii *et al* in [65], where the authors reported similar results with respect to the one presented for UVB LEDs.

In addition to the mechanisms described above, device aging can also include spatial non-uniformities in the emission of UV LEDs. Ruschel *et al* found a reduction in the homogeneity of the spatial EL intensity distribution of a 310 nm LED during a constant current stress at 200 A cm^{-2} and at a temperature of $T_{hs} \approx 29$ °C [66]. At the beginning of long-term operation, the EL intensity showed an almost homogeneous distribution (figure 43(a)). Long-term operation resulted in areas *ALC* with greatly reduced EL intensity and areas *AHC* with high EL intensities, that are partly even higher than at the beginning (figure 43(b)). The homogeneity of the corresponding PL intensity distribution decreased in a similar way, but the intensity patterns are complementary to the EL intensity patterns. Thus, the authors concluded that the current density distribution changed during operation. Moreover, the authors proved that the active region degrades more rapidly in areas where a higher current density flows. The results were supported by time-resolved PL measurements, which revealed that the charge carrier lifetimes and thus the radiative recombination rate decreases in the active region during operation. The change in the intensity distribution was explained by a self-amplifying process, which leads to a spatially non-uniform p-side conductivity. This results in a non-uniform current distribution, which in turn can influence the degradation dynamics. In this context, it has been suggested that breaking of Mg–H complexes and subsequent migration of hydrogen in the structure plays an important role [54, 67]. Furthermore, the spatial distributions of the EL intensity could be related to the p-side acceptor concentration has already been concluded for InGaN-based blue LEDs [68].

3.2.3. Overview of recent reports in the field of UV LED reliability

In this paper, we analyze the degradation models proposed in literature for UV LEDs, explaining in detail their characteristics and their extraction from the experimental measurements. It is worth noticing that, beyond the papers already cited in the previous sections, several other works gave an important contribution to the knowledge of the degradation mechanisms on UVC LEDs. This section summarizes the most important reports, to give a comprehensive overview of the topic.

Additional evidence about the generation of defects during aging were provided by Wang *et al* in [67]. Specifically, the authors used PL measurements to identify defects generated in a 272 nm UVC LED during aging. The authors found an increase in the defect-related emission peak at 515 nm, which is typically attributed to radiative transitions mediated by Ga vacancies. By using C-DLTS measurements (results in figure 44), the authors were able to correlate the reduction in the amplitude of a negative peak 'A' with the increase in the positive peak 'B', demonstrating a linear relationship between defect density and the decrease in optical power. By combining these results with DFT and SIMS measurements, the authors ascribed the departure of Mg from Mg_{Ga} complexes along dislocations as the cause of the generation of gallium vacancies during the stress.

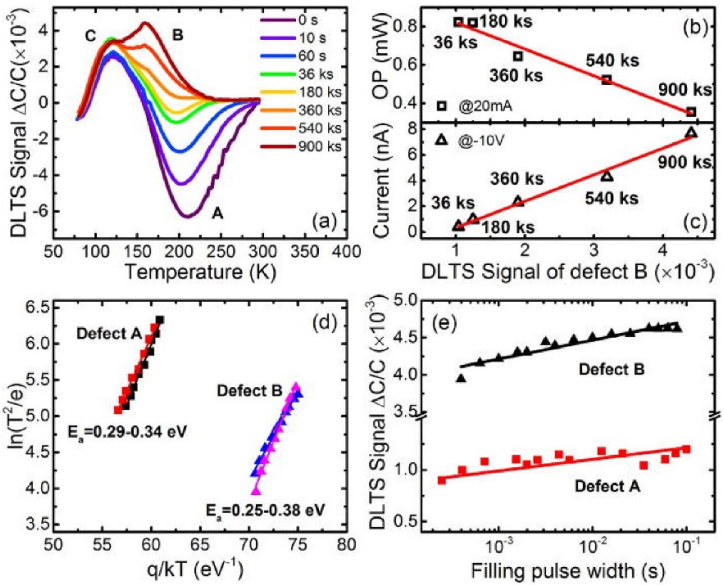

Figure 44. (a) C-DLTS spectra of 272 nm LED (Vbias = −6 V, Vfill = −2 V); (b) and (c) Correlation between the *OP*, the C-DLTS signal of defect 'B' during the stress, and the sub-threshold leakage current; (d) Arrhenius plot of the founded defects; (e) Capture kinetics for defects 'A' and 'B'. Reprinted from [67], with the permission of AIP Publishing.

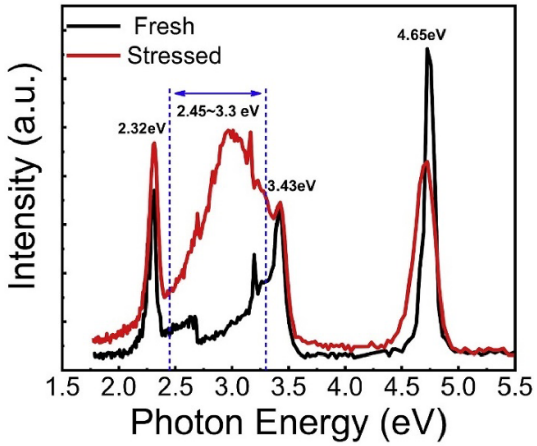

Figure 45. Comparison of the cathodoluminescence spectra before and after the stress test on a DUV LED, measured with an electron accelerating voltage of 7 kV. Reprinted from [69], Copyright (2020), with permission from Elsevier.

Signatures of defects generation during stress were also identified by Ma *et al* in [69], where the authors employed cathodoluminescence (CL) measurements on a 265 nm LED to identify the regions where defects are generated after the aging. As reported in figure 45, they found that the majority of the collected CL signals are from the regions above the MQWs, and they correlated the emission in the energy range of 2.45–3.30 eV with the generation of point defects in the QW area during the stress test, in particular in the first QW near the p-side.

Continuing with studies regarding the generation of defects in AlGaN-based UVC LEDs, Polyakov *et al* [70] introduced defects in their 270 nm devices with proton irradiation, which increased their series resistance, decreased the charge density in QWs, and led to the appearance of two defects traps at $\mathbf{E}_c$-0.5 eV and E_c-0.35 eV, observed through C-DLTS measurements. This second defect trap was also identified as an electron trap in the QWs. Moreover, the authors noticed a possible defect rearrangement in the potential fluctuation in the active region caused by electron irradiation and the excess of charge carriers, which led to an increase in the leakage current in the LED. They also concluded that the AlGaN-based DUV LEDs are more tolerant to 5 MeV electron radiation than their InGaN-based counterpart, used for visible LEDs, because of the higher bond strengths in high Al mole fraction AlGaN. About the same topic, regarding the defect generation, Li *et al* presented similar results in [71], where they described an increase in leakage

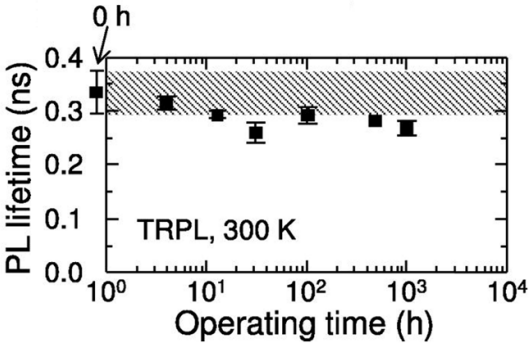

Figure 46. Time resolved photoluminescence lifetimes calculated at room temperature as a function of the operating time. Reprinted from [44], with the permission of AIP Publishing.

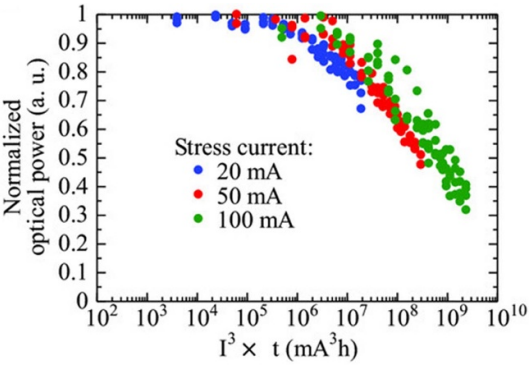

Figure 47. Lifetime results of 230 nm LEDs in function of the cubed of the stress current with time [74]. John Wiley & Sons. © 2024 Wiley-VCH GmbH.

current caused by the increase in TAT processes after the irradiation. Here, the authors also identified the generation of deep-levels in proximity of the EBL and the interlayer.

In [44] Chichibu *et al* analyzed the PL decay time (τ_{PL}) of 275 nm LEDs, which corresponds approximately to the lifetime of the minority carriers at low excitation, as a function of the stress time. They concluded that the observed reduction in τ_{PL} (see figure 46) is too small to entirely explain the decrease in the optical power (40% after 1002 h) by a decreasing IQE in the quantum wells. Therefore, the authors attributed the degradation to the decrease in injection efficiency in the active region, as pointed out in section 3.2.2. The fact that the reduction in the PL decay time is too small to attribute the operation-induced reduction in the optical power (EL measurement) solely to the increasing non-radiative recombination rate in the active region was also observed with 310 nm LEDs in [66]. However, this discrepancy between PL and EL could be explained there by the fact that the active region has aged spatially inhomogeneously (see figure 43). Accordingly, the measured PL signal also partly consists of components from areas that have not aged, which means that the change in the measured PL decay time is lower overall. In contrast to the study [44], the study [66] concludes that the increase in the non-radiative recombination rate in the active region may be the main loss mechanism of degradation. However, it cannot be ruled out that several loss mechanisms are responsible for the degradation and that these vary from LED to LED.

Other results that supported the hypotheses and the models proposed in previous paragraphs were shown in [72] and in [73], where Su and Liu and Loveless *et al* presented a study on the degradation mechanisms and on the performance of commercial UVC LEDs, respectively.

Moving towards shorter wavelengths, Kobayashi *et al* [74] investigated the lifetime of far UVC LEDs, in the range between 226–240 nm, reporting an estimated L70 of 11 000 h and L50 of 28 000 h, extracted with the formula proposed in [34]. They also confirmed the J^3 dependency of optical power degradation with stress time for UVC devices, reported in figure 47 as shown in [21] for UVB samples. Finally, Kobayashi *et al* [74] in their work demonstrated the progress of solid-state far UVC emitters with respect to [75], where Yoshikawa *et al* determined a lifetime for 233 nm LEDs as 3600 h.

Lastly, Letson *et al* [76] provided a conspicuous analysis of the lifetime of commercial UVC LEDs, concluding that at the state-of-the-art they are ready to replace mercury-vapor lamps as UV light sources for contactless discharge of surfaces during scientific missions in space.

4. Summary, conclusions and guidances

UVC LEDs are a rapidly expanding technology, based on AlGaN semiconductor materials, that offer the promise of new capabilities and applications for UVC sources that are not possible with conventional UV technologies, such as mercury discharge lamps. While the AlGaN-based semiconductors used in UVC LED products may have benefited from the recent advancement of InGaN-based LED products that are used in lighting applications, the performance and reliability of commercially-available devices based on the two families of semiconductor materials exhibit consistent differences. The goal of this review is to increase the awareness of those differences by discussing the performance of AlGaN UV LEDs through the sharing of findings from extensive testing of commercial products from 15 different manufacturers—which are representative of typical UV LEDs—from various countries of origin (including the United States of America, South Korea, China, and Japan), with different templates for the semiconductor layer structure, and different packaging technologies. Additionally, with particular relation to commercial devices, we also outline the major drawbacks of such technology, including an in-depth overview on temperature sensitivity of UVC LEDs, their lifetime-limiting physical processes and on the peculiar packaging required to sustain both high-energy UV photons and high localized self-heating.

We found the characteristics of commercial UVC LEDs to vary widely, with emission wavelengths between 265 and 283 nm producing radiant powers between 10 and >150 mW. In general, higher radiant powers were observed for LEDs emitting at longer wavelengths (i.e. 275 nm and above). The radiant power of some UVC LEDs was found to scale approximately linearly with current at room temperature, although there were a significant number of products that exhibited faster thermal droop at lower currents, resulting in a non-linear response at high operating temperatures. This finding is a consequence of the wide variation in WPE observed for the tested products, with the best UVC LEDs exhibiting WPE values of 7.5% at an emission wavelength of 275 nm. In contrast, the WPE of the least efficient products were approximately 2%. Improving WPE enables the LED to deliver higher radiant powers at lower operating currents and with reduced energy consumption and heat loss.

It was found that the temperature dependence of the radiant power can be different for LEDs of different manufacturers and ranges from −0.8%/K to +0.4%/K. The LEDs can also differ slightly in their linearity of the radiant power vs. current characteristic. Particularly at low currents, a change in the linearity of the radiant power curve was frequently observed in the LEDs of various manufacturers during long-term operation. The latter effect influences the dimmability of UVC LEDs. The current and temperature dependence of the radiant power is mainly due to non-radiative recombination processes (e.g. SRH recombination, Auger–Meitner recombination) affecting the IQE, as well as to limitations in carrier injection. The SRH recombination rate is likely dominant at lower current densities while Auger–Meitner recombination plays an essential role at higher current densities. Nevertheless, self-heating at high currents can also have a strong influence, as non-radiative recombination rates (e.g. SRH recombination) increase with higher temperatures. As a matter of fact, the combined low optical efficiency and high electrical power required to drive AlGaN-based LEDs result in a much higher power dissipation, compared to shorter-wavelength emitters. Therefore, for an equivalent package footprint, more efficient thermal solutions have to be embedded by the manufacturers to allow adequate disposal of waste power in the form of heat. Additionally, if a high irradiance needs to be achieved at system-level, also the thermal management solution of the luminaire needs to be designed accordingly, considering that it may have to deal with heat power densities much higher compared to visible LEDs.

From a user perspective, significant variation in non-linearity and drift in thermal stability in combination with lower efficiency observed in UVC LED products in comparison with visible LEDs could lead to less predictable and less optimal operational performance in applications. That, in turn, could result in either underperforming and dissatisfactory disinfection devises or more expensive UVC LED-based systems, which are over-designed in order to overcome observed variations in UVC LED performance at different application operating conditions and over time.

The reliability of UVC LEDs is affected by gradual degradation (also referred to as radiant flux depreciation) and by sudden CFs. While all UVC LED products exhibited gradual radiant power degradation at varying rates over extended times, CFs tended to be more likely in selected products. Some UVC LEDs operated for up to 10 000 h and still maintained >90% of the initial radiant power (R90 ⩾ 10 000 h). However, other LEDs degraded faster, and their radiant power dropped below 90% after 100 h (see section 2.2.2). Temperature and current density were found to have the highest impact on the gradual

degradation with higher temperature and/or higher current densities leading to shorter lifetimes (see section 2.2.3). It is therefore not recommended to operate such devices under maximum current and or maximum temperature conditions for long periods. It is assumed that the increase in the concentration of NRRCs is a cause of the decrease of the radiant power over time. However, there are also indications that a deterioration of charge CIE also contributes to the decrease in radiant power. Additionally, we also showed that the lifetime of UVC LEDs can also be limited by the robustness of the packaging materials against high energy-radiation. While improvements in these fields will strongly depend on technological advancements, end users should be aware that also the optics of the luminaire system can easily degrade when exposed to UVC radiation for prolonged periods. Therefore, it is advisable to select materials with proved robustness against the specific light, in terms of photon energy and density, that is being generated by the system.

Furthermore, this review paper also deals with the mathematical description and extrapolation of the temporal course of the radiation power during long-term operation. In contrast to visible solid-state emitters, where a classical exponential function has been typically used to model the trend of the relative flux depreciation [28, 29], recent works demonstrated that purely exponential decays do not represent the best mathematical description in the case of UVC and UVB LEDs. Nevertheless, section 3.1 provides an overview of descriptive models that can partially describe such curve progressions well.

In addition to the change in the current dependency of the radiant power (described above), a change in the temperature dependency of the radiation power after long-term operation was also observed in several UVC LEDs. This can lead to deviations if the temporal course of the radiant power is recorded under a specific measurement condition that deviates from the operating condition in the long-term experiment. It is therefore recommended to follow the recommendations of LM-80-21 [29], which state that 'measurement current should be equal to test stress current'. However, since the temperature dependency of the radiant power can also change, it may also be important that the measuring temperature corresponds to the stress temperature, which is strongly related to the specific use case and operating profile. Therefore, the measurement conditions must be adapted to the stress conditions if the lifetime of a UVC LED is to be determined in a specific application. Generally speaking, potential users should be aware that radiant power maintenance models typically used to predict the lifetime of visible LEDs will fail in estimating the useful operating life of a UVC LED. This ultimately suggests that the scientific and industrial community should take action and begin consolidating new measuring and analysis approaches specifically devoted to this class of rapidly emerging solid-state emitters. This would allow to provide a more comprehensive and shared knowledge base to both device manufacturers and users, ultimately defining the additional set of data required for a correct evaluation of UVC LEDs performance and lifetime.

To conclude, it has been shown that efficiency and lifetime of UVC LEDs depend strongly on operation conditions, which has to be considered for designing of UVC LED-based systems. As new technological solutions become available, it is expected that some of the issues presented in this paper will be solved, or at least mitigated. Nevertheless, UVC LEDs specific behaviors—such as unconventional radiant power decay trends, the emission of high-energy photons, increased self-heating and temperature sensitivity—will have to be handled by the final user, whom should be properly made aware of the substantial differences that discriminated UVC LEDs from visible solid-state sources.

Data availability statement

The data cannot be made publicly available upon publication due to legal restrictions preventing unrestricted public distribution. The data that support the findings of this study are available upon reasonable request from the authors.

Acknowledgments

The authors thank Johannes Glaab (FBH) for the contribution in carrying out aging experiments and for providing SIMS data. The work was partially supported within the DINoLED project of the German Federal Ministry for Economic Affairs and Climate Action under Contract 03TN0024B within the WIPANO program for knowledge and technology transfer via patents and standards. This work was also partially funded under the National Recovery and Resilience Plan (NRRP), Mission 4, Component C2, Investment 1.1, by the European Union—NextGenerationEU. PRIN Project 20225YYLEP, CUP: C53D23000350006, 'Empowering UV Led technologies for high-efficiency disinfection: from semiconductor-level research to SARs-Cov-2 inactivation' (D.D. 104-02/02/2022 Ministero dell'Università e della Ricerca). This manuscript reflects only the authors' views and opinions and the Ministry cannot be considered responsible for them.

References

[1] Kneissl M, Seong T-Y, Han J and Amano H 2019 The emergence and prospects of deep-ultraviolet light-emitting diode technologies *Nat. Photon.* **13** 233–44
[2] Kneissl M and Rass J (eds) 2016 *III-Nitride Ultraviolet Emitters* (*Springer Series in Materials Science*) vol 227 (Springer)
[3] Peng Y, Liang R, Mou Y, Dai J, Chen M and Luo X 2019 Progress and perspective of near-ultraviolet and deep-ultraviolet light-emitting diode packaging technologies *J. Electron. Packag.* **141** 040804
[4] De Santi C, Caria A, Piva F, Meneghesso G, Zanoni E and Meneghini M 2021 Degradation mechanisms of InGaN visible LEDs and AlGaN UV LEDs *Reliability of Semiconductor Lasers and Optoelectronic Devices* (Woodhead Publishing) pp 273–312
[5] Mondal R K, Adhikari S, Chatterjee V and Pal S 2021 Recent advances and challenges in AlGaN-based ultra-violet light emitting diode technologies *Mater. Res. Bull.* **140** 111258
[6] Herzog A, Benkner S, Zandi B, Buffolo M, Van Driel W D, Meneghini M and Khanh T Q 2023 Lifetime prediction of current-and temperature-induced degradation in silicone-encapsulated 365 nm high-power light-emitting diodes *IEEE Access* **11** 19928–40
[7] Grandusky J R, Gibb S R, Mendrick M C, Moe C, Wraback M and Schowalter L J 2011 High output power from 260 nm pseudomorphic ultraviolet light-emitting diodes with improved thermal performance *Appl. Phys. Express* **4** 082101
[8] Shatalov M *et al* 2012 AlGaN deep-ultraviolet light-emitting diodes with external quantum efficiency above 10% *Appl. Phys. Express* **5** 082101
[9] Kowalski W 2009 Ultraviolet germicidal irradiation handbook: UVGI for air and surface disinfection *Ultraviolet Germicidal Irradiation Handbook: UVGI for Air and Surface Disinfection* (Springer) pp 1–501
[10] Ratliff K, Oudejans L, Calfee W, Abdel-Hady A, Monge M and Aslett D 2022 Evaluating the impact of ultraviolet C exposure conditions on coliphage MS2 inactivation on surfaces *Lett. Appl. Microbiol.* **75** 933–41
[11] Schubert E F 2006 Light-emitting diodes *Light-Emitting Diodes* vol 9780521865388 (Cambridge University Press), 2nd edn pp 1–422
[12] Damilano B and Gil B 2015 Yellow–red emission from (Ga,In)N heterostructures *J. Phys. D: Appl. Phys.* **48** 403001
[13] Kolbe T, Mehnke F, Guttmann M, Kuhn C, Rass J, Wernicke T and Kneissl M 2013 Improved injection efficiency in 290 nm light emitting diodes with Al(Ga)N electron blocking heterostructure *Appl. Phys. Lett.* **103** 31109
[14] Lee K H, Park H J, Kim S H, Asadirad M, Moon Y-T, Kwak J S and Ryou J-H 2015 Light-extraction efficiency control in AlGaN-based deep-ultraviolet flip-chip light-emitting diodes: a comparison to InGaN-based visible flip-chip light-emitting diodes *Opt. Express* **23** 20340–9
[15] Cao X A, LeBoeuf S F and Stecher T E 2006 Temperature-dependent electroluminescence of AlGaN-based UV LEDs *IEEE Electron Device Lett.* **27** 329–31
[16] Moe C G *et al* 2012 Impact of temperature-dependent hole injection on low-temperature electroluminescence collapse in ultraviolet light-emitting diodes *Appl. Phys. Lett.* **101** 43
[17] De Santi C *et al* 2017 Recombination mechanisms and thermal droop in AlGaN-based UV-B LEDs *Photon. Res.* **5** A44–A51
[18] Chen J *et al* 2023 Hillock related degradation mechanism for AlGaN-based UVC LEDs *Nanomaterials* **13** 1562
[19] Buffolo M, Meneghini M, Munaretto A, De Santi C, Meneghesso G and Zanoni E 2017 Failure of high power LEDs submitted to EOS: dependence on device layout and pulse properties *IEEE Trans. Device Mater. Reliab.* **17** 191–6
[20] Buffolo M, Davanzo E, De Santi C, Trivellin N, Meneghesso G, Zanoni E and Meneghini M 2020 Efficiency and catastrophic failure of high-power blue GaN LEDs during extremely high temperature and current stress *IEEE Trans. Device Mater. Reliab.* **20** 429–35
[21] Ruschel J, Glaab J, Beidoun B, Ploch N L, Rass J, Kolbe T, Knauer A, Weyers M, Einfeldt S and Kneissl M 2019 Current-induced degradation and lifetime prediction of 310 nm ultraviolet light-emitting diodes *Photon. Res.* **7** B36–B40
[22] Herzog A, Wagner M and Khanh T Q 2020 Efficiency droop in green InGaN/GaN light emitting diodes: degradation mechanisms and initial characteristics *Microelectron. Reliab.* **112** 113792
[23] Fujioka A, Asada K, Yamada H, Ohtsuka T, Ogawa T, Kosugi T, Kishikawa D and Mukai T 2014 High-output-power 255/280/310 nm deep ultraviolet light-emitting diodes and their lifetime characteristics *Semicond. Sci. Technol.* **29** 084005
[24] Piva F, Buffolo M, De Santi C, Meneghesso G, Zanoni E, Meneghini M and Trivellin N 2023 Status of performance and reliability of 265 nm commercial UV-C LEDs in 2023 *IEEE Trans. Electron Devices* **70** 5696–700
[25] Lu C-C, Wang C-P, Liu C-Y and Hsu C-P 2016 The efficiency and reliability improvement by utilizing quartz airtight packaging of UVC LEDs *IEEE Trans. Electron Devices* **63** 3143–6
[26] Nagasawa Y and Hirano A 2019 Review of encapsulation materials for AlGaN-based deep-ultraviolet light-emitting diodes *Photon. Res.* **7** B55–B65
[27] Yen H-H, Kuo H-C and Yeh W-Y 2010 Particular failure mechanism of gan-based alternating current light-emitting diode induced by GaO_x Oxidation *IEEE Photonics Technol. Lett.* **22** 1168–70
[28] ANSI/IES TM-21-21 Technical memorandum: projecting long-term luminous, photon, and radiant flux maintenance of LED light sources (available at: https://webstore.ansi.org/standards/iesna/ansiiestm21?srsltid=AfmBOoopviG2jRIwh1sVu4kIV9VQe1gXwipcJzGSn8rQowfNtNN3Ffcc) (Accessed 19 March 2025)
[29] ANSI/IES LM-80-21 Approved method: measuring maintenance of light output characteristics of solid-state light sources (available at: https://webstore.ansi.org/standards/iesna/ansiieslm8021?srsltid=AfmBOoqsIpm0D1ouPv6sboMr0dQYFwB_U-3HhKmw-iDnlD4lLsqmjPAE) (Accessed 19 March 2025)
[30] Iveland J, Martinelli L, Peretti J, Speck J S and Weisbuch C 2013 Direct measurement of auger electrons emitted from a semiconductor light-emitting diode under electrical injection: identification of the dominant mechanism for efficiency droop *Phys. Rev. Lett.* **110** 177406
[31] Kioupakis E, Yan Q, Steiauf D and Van De Walle C G 2013 Temperature and carrier-density dependence of Auger and radiative recombination in nitride optoelectronic devices *New J. Phys.* **15** 125006
[32] Piva F, De Santi C, Deki M, Kushimoto M, Amano H, Tomozawa H, Shibata N, Meneghesso G, Zanoni E and Meneghini M 2020 Modeling the degradation mechanisms of AlGaN-based UV-C LEDs: from injection efficiency to mid-gap state generation *Photon. Res.* **8** 1786–91
[33] Gesztelyi R, Zsuga J, Kemeny-Beke A, Varga B, Juhasz B and Tosaki A 2012 The Hill equation and the origin of quantitative pharmacology *Arch. Hist. Exact Sci.* **66** 427–38
[34] Zhang J, Zhou L, Gao Y, Lunev A, Zhang B and Wu S 2023 Defect dynamics and internal quantum efficiency decay resultant ultraviolet C-band light-emitting diode lifetime performance *Phys. Status Solidi a* **220** 2200433
[35] Piva F *et al* 2023 Impact of Mg-doping on the performance and degradation of AlGaN-based UV-C LEDs *Appl. Phys. Lett.* **122** 151108

[36] Uematsu M and Wada K 1992 Time dependence of recombination-enhanced impurity diffusion in GaAs *Appl. Phys. Lett.* **60** 1612–4
[37] Kimerling L C 1978 Recombination enhanced defect reactions *Solid State Electron.* **21** 1391–401
[38] Meneghini M, Dal Lago M, Trivellin N, Mura G, Vanzi M, Meneghesso G and Zanoni E 2012 Chip and package-related degradation of high power white LEDs *Microelectron. Reliab.* **52** 804–12
[39] Renso N, De Santi C, Caria A, Dalla Torre F, Zecchin L, Meneghesso G, Zanoni E and Meneghini M 2020 Degradation of InGaN-based LEDs: demonstration of a recombination-dependent defect-generation process *J. Appl. Phys.* **127** 185701
[40] De Santi C, Caria A, Renso N, Dogmus E, Zegaoui M, Medjdoub F, Meneghesso G, Zanoni E and Meneghini M 2018 Evidence of optically induced degradation in gallium nitride optoelectronic devices *Appl. Phys. Express* **11** 111002
[41] Kolbe T, Knauer A, Ruschel J, Rass J, Kyong Cho H, Hagedorn S, Glaab J, Lobo Ploch N, Einfeldt S and Weyers M 2021 Comparison of ultraviolet B light-emitting diodes with single or triple quantum wells *Phys. Status Solidi a* **218** 2100100
[42] Gong Z, Gaevski M, Adivarahan V, Sun W, Shatalov M and Asif Khan M 2006 Optical power degradation mechanisms in AlGaN-based 280 nm deep ultraviolet light-emitting diodes on sapphire *Appl. Phys. Lett.* **88** 121106
[43] Meneghini M, Trevisanello L-R, Meneghesso G and Zanoni E 2008 A review on the reliability of GaN-based LEDs *IEEE Trans. Device Mater. Reliab.* **8** 323–31
[44] Chichibu S F, Nagata K, Oya M, Kasuya T, Okuno K, Ishiguro H, Saito Y, Takeuchi T and Shima K 2023 Operation-induced degradation mechanisms of 275 nm-band AlGaN-based deep-ultraviolet light-emitting diodes fabricated on a sapphire substrate *Appl. Phys. Lett.* **122** 201105
[45] Nykänen H, Suihkonen S, Kilanski L, Sopanen M and Tuomisto F 2012 Low energy electron beam induced vacancy activation in GaN *Appl. Phys. Lett.* **100** 122105
[46] Huang C-Y, Hsieh W-H, Shao T-L, Wu C-H and Lu T-C 2023 Degradation of high-power UVC light-emitting diodes via emission-activated nitrogen vacancy generation *IEEE Trans. Electron Devices* **70** 3166–71
[47] Puzyrev Y S, Roy T, Beck M, Tuttle B R, Schrimpf R D, Fleetwood D M and Pantelides S T 2011 Dehydrogenation of defects and hot-electron degradation in GaN high-electron-mobility transistors *J. Appl. Phys.* **109** 34501
[48] Roccato N *et al* 2023 Modeling the electrical degradation of AlGaN-based UV-C LEDs by combined deep-level optical spectroscopy and TCAD simulations *Appl. Phys. Lett.* **122** 161105
[49] Buffolo M, Caria A, Piva F, Roccato N, Casu C, De Santi C, Trivellin N, Meneghesso G, Zanoni E and Meneghini M 2022 Defects and reliability of GaN-based LEDs: review and perspectives *Phys. Status Solidi a* **219** 2100727
[50] Reshchikov M A 2021 Measurement and analysis of photoluminescence in GaN *J. Appl. Phys.* **129** 121101
[51] Polyakov A Y and Lee I H 2015 Deep traps in GaN-based structures as affecting the performance of GaN devices *Mater. Sci. Eng. R* **94** 1–56
[52] Bisi D, Meneghini M, De Santi C, Chini A, Dammann M, Bruckner P, Mikulla M, Meneghesso G and Zanoni E 2013 Deep-level characterization in GaN HEMTs-part I: advantages and limitations of drain current transient measurements *IEEE Trans. Electron Devices* **60** 3166–75
[53] Piva F *et al* 2023 Degradation of AlGaN-based UV-C SQW LEDs analyzed by means of capacitance deep-level transient spectroscopy and numerical simulations *Appl. Phys. Lett.* **122** 181102
[54] Glaab J *et al* 2019 Degradation of (In)AlGaN-Based UVB LEDs and migration of hydrogen *IEEE Photonics Technol. Lett.* **31** 529–32
[55] Hacke P, Nakayama H, Detchprohm T, Hiramatsu K and Sawaki N 1996 Deep levels in the upper band-gap region of lightly Mg-doped GaN *Appl. Phys. Lett.* **68** 1362–4
[56] Polyakov A Y, Smirnov N B, Govorkov A V, Kozhukhova E A, Dabiran A M, Chow P P, Wowchak A M, Lee I-H, Ju J-W and Pearton S J 2009 Comparison of electrical properties and deep traps in p-$Al_xGa_{1-x}N$ grown by molecular beam epitaxy and metal organic chemical vapor deposition *J. Appl. Phys.* **106** 73706
[57] Duc T T, Pozina G, Janzén E and Hemmingsson C 2013 Investigation of deep levels in bulk GaN material grown by halide vapor phase epitaxy *J. Appl. Phys.* **114** 153702
[58] Auf Der Maur M, Galler B, Pietzonka I, Strassburg M, Lugauer H and Di Carlo A 2014 Trap-assisted tunneling in InGaN/GaN single-quantum-well light-emitting diodes *Appl. Phys. Lett.* **105** 133504
[59] Pant N, Bushick K, McAllister A, Lee W, Van de Walle C G and Kioupakis E 2024 Carrier confinement and alloy disorder exacerbate Auger-Meitner recombination in AlGaN ultraviolet light-emitting diodes *Appl. Phys. Lett.* **125** 021109
[60] Strauss U, Lermer T, Müller J, Hager T, Brüderl G, Avramescu A, Lell A and Eichler C 2012 Study of defects and lifetime of green InGaN laser diodes *Phys. Status Solidi a* **209** 481–6
[61] Susilo N *et al* 2020 Improved performance of UVC-LEDs by combination of high-temperature annealing and epitaxially laterally overgrown AlN/sapphire *Photon. Res.* **8** 589–94
[62] Meneghini M, De Santi C, Tibaldi A, Vallone M, Bertazzi F, Meneghesso G, Zanoni E and Goano M 2020 Thermal droop in III-nitride based light-emitting diodes: physical origin and perspectives *J. Appl. Phys.* **127** 211102
[63] Chichibu S, Sota T, Wada K and Nakamura S 1998 Exciton localization in InGaN quantum well devices *J. Vac. Sci. Technol. B* **16** 2204–14
[64] Piva F, De Santi C, Deki M, Kushimoto M, Amano H, Tomozawa H, Shibata N, Meneghesso G, Zanoni E and Meneghini M 2019 Stability and degradation of AlGaN-based UV-B LEDs: role of doping and semiconductor defects *Microelectron. Reliab.* **100–101** 113418
[65] Ishii R, Yoshikawa A, Nagase K, Funato M and Kawakami Y 2020 Temperature-dependent electroluminescence study on 265 nm AlGaN-based deep-ultraviolet light-emitting diodes grown on AlN substrates *AIP Adv.* **10** 125014
[66] Ruschel J, Tomm J W, Glaab J, Kolbe T, Knauer A, Rass J, Lobo-Ploch N, Musengezi T A and Einfeldt S 2023 Spatially resolved degradation effects in UVB LEDs stressed by constant current operation *Appl. Phys. Lett.* **122** 131103
[67] Wang Y-Z *et al* 2020 Degradation in AlGaN-based UV-C LEDs under constant current stress: a study on defect behaviors *Appl. Phys. Lett.* **116** 33
[68] Onushkin G A, Hong S-S, Lee J-H, Park J-S, Son J-K, Kim M-H and Park Y 2009 Local electroluminescence and time-resolved photoluminescence study of InGaN light-emitting diodes *Appl. Phys. Lett.* **95** 45
[69] Ma Z *et al* 2020 The influence of point defects on AlGaN-based deep ultraviolet LEDs *J. Alloys Compd.* **845** 156177
[70] Polyakov A Y *et al* 2024 Point defect effects in AlGaN 270 nm light emitting diodes introduced by MeV electron and proton irradiation *APL Mater.* **12** 59
[71] Li J-S, Chiang C-C, Wan H-H, Kim J, Barke S, Wass P, Ren F, Conklin J W and Pearton S J 2024 MeV proton and neutron damage effects on deep-ultraviolet light-emitting diodes *J. Vac. Sci. Technol. B* **42** 52206
[72] Su M and Liu H 2024 Effect of trap behavior on recombination in AlGaN-based UV-C LEDs degradation *IEEE Trans. Electron Devices* **71** 1974–9

[73] Loveless J, Kirste R, Moody B, Reddy P, Rathkanthiwar S, Almeter J, Collazo R and Sitar Z 2023 Performance and reliability of state-of-the-art commercial UVC light emitting diodes *Solid State Electron.* **209** 108775
[74] Kobayashi H, Sato K, Okuaki Y, Lee T G, Kunimi Y and Kuze N 2024 Enhanced wall-plug efficiency over 2.4% and wavelength dependence of electrical properties at far UV-C light-emitting diodes on single-crystal AlN substrate *Phys. Status Solidi (RRL)* **18** 2400002
[75] Yoshikawa A, Hasegawa R, Morishita T, Nagase K, Yamada S, Grandusky J, Mann J, Miller A and Schowalter L J 2020 Improve efficiency and long lifetime UVC LEDs with wavelengths between 230 and 237 nm *Appl. Phys. Express* **13** 022001
[76] Letson B C, Barke S, Wass P, Mueller G, Ren F, Pearton S J and Conklin J W 2023 Deep UV AlGaN LED reliability for long duration space missions *J. Vac. Sci. Technol. A* **41** 13202